Loss-of-Function *DESI1* Variants

Cause a Novel ALS-like Syndrome

by

Seyide Ecesu Uygur

A Dissertation Submitted to the
Graduate School of Health Sciences
in Partial Fulfillment of the Requirements for
the Degree of

Master of Science

in

Cellular and Molecular Medicine

KOÇ
ÜNİVERSİTESİ

September 18, 2025

Loss-of-Function *DESI1* Variants Cause a Novel ALS-like Syndrome

Koç University

Graduate School of Health Sciences

This is to certify that I have examined this copy of a master's thesis by

Seyide Ecesu Uygur

and have found that it is complete and satisfactory in all respects,
and that any and all revisions required by the final
examining committee have been made.

Committee Members:

_____

Assist. Prof. Nathalie Escande-Beillard, PhD (Advisor)

_____

Assoc. Prof. Atay Vural, MD, PhD

_____

Assoc. Prof. Umut Şahin, PhD

Date: _____

ABSTRACT

Loss-of-Function *DESI1* Variants Cause a Novel ALS-like Syndrome

Seyide Ecesu Uygur

Master of Science in Cellular and Molecular Medicine

September 18, 2025

Neurodegenerative diseases encompass a diverse group of disorders characterized by progressive and irreversible neuronal damage. Among them, amyotrophic lateral sclerosis (ALS) is the most common motor neuron disease, defined by progressive degeneration of upper and lower motor neurons.

ALS has a multifactorial aetiology shaped by complex interaction between genetic and environmental factors, with about 20% of cases explained by monogenic causes. To date, pathogenic variants in more than 40 genes have been identified. Notably, several ALS-associated genes including *SOD1*, *TARDBP* as well as *UBQLN* family members, converge on proteostasis pathways, a major hallmark in ALS pathophysiology. Yet nearly 80% of patients still lack a molecular diagnosis, highlighting the critical need for continued genetic investigation.

Through international collaboration, we identified seven patients from six unrelated families presenting with ALS-like phenotypes. Despite their diverse geographic origins, all individuals exhibited hallmark clinical features, most notably progressive weakness and combined involvement of upper and lower motor neurons.

Whole-exome sequencing (WES) excluded pathogenic variants in known neuromuscular disease genes but revealed novel homozygous or compound heterozygous variants in *Desumoylating Isopeptidase 1* (*DESI1*). These included three splice-site, two frameshift, and one nonsense mutations. All variants were extremely rare in the general population and segregated consistently with autosomal recessive inheritance.

DESI1 encoding a protein with a conserved cysteine protease PPPDE domain and nuclear export signals (NES), acts as an adaptor for the nuclear export of UBQLN proteins. Previously not associated with human disease, *DESI1* emerges as a novel ALS candidate linking nuclear transport defects to proteostasis disruption.

To assess the functional consequences of these variants, we overexpressed *DESI1* variants in HEK293T cells. Splicing and immunoblotting assays revealed truncated or aberrant proteins lacking essential domains, including the highly conserved catalytic cysteine residue and nuclear export signals. Western blot analysis showed that these proteins undergo rapid proteasomal degradation. Co-immunoprecipitation further revealed abnormal interactions with UBQLN4 and impaired deSUMOylase activity toward BZEL, the only known substrate. Preliminary analyses on patient-derived fibroblasts supported these findings, revealing impaired proteostasis.

Together, these findings establish *DESI1* as a novel ALS-associated gene and demonstrate that loss-of-function variants provide mechanistic insights linking its dysfunction to ALS pathogenesis.

ÖZETÇE

Fonksiyon Kaybı *DESI1* Varyantları Yeni Bir ALS Benzeri Sendroma Neden Olmaktadır

Seyide Ecesu Uygur

Hücresel ve Moleküler Tıp Yüksek Lisans

Eylül 18, 2025

Nörodejeneratif hastalıklar, ilerleyici ve geri döndürülemez sinir hasarıyla karakterize bir hastalık grubudur. Bu grup içinde en yaygın motor nöron hastalığı olan amiyotrofik lateral skleroz (ALS), üst ve alt motor nöron dejenerasyonu ile tanımlanır.

ALS, genetik ve çevresel faktörlerin etkileşimiyle gelişen kompleks bir hastalıktır. Vakaların yaklaşık %20'si monogenik varyantlarla ilişkilendirilmiş olup, bugüne kadar 40'tan fazla gende patojenik varyant tanımlanmıştır. Çok sık rastlanan SOD1, TARDBP'nin yanı sıra UBQLN2 gibi UBQLN ailesi üyeleri de ALS patomekanizmasının temelinde olan proteostaz bozukluğunda birleşmektedir. Bununla birlikte, olguların yaklaşık %80'inde hâlâ moleküler tanı konulamaması, genetik araştırmaların sürdürülmesini kritik kılmaktadır.

Uluslararası iş birliklerimiz kapsamında, "ALS benzeri" klinik fenotipe sahip altı farklı aileden yedi hasta tanımladık. Farklı coğrafi kökenleri olan bu hastalarda ilerleyici güçsüzlük ile üst-alt motor nöron tutulumu gözlendi. Etkilenen bireylerde tüm ekzom dizileme (WES) ile bilinen nöromüsküler hastalık genlerindeki varyantlar dışlandı; ancak daha önce hiçbir hastalıkla ilişkilendirilmemiş Desumoylating Isopeptidase 1 (DESI1) geninde homozigot veya bileşik heterozigot varyantlar tespit edildi. Bu varyantlar arasında üç splice-site, iki çerçeve kayması ve bir anlamsız mutasyon bulunmakta olup, hepsi genel popülasyonda nadir olan allellerdi. Varyantlar otozomal resesif kalıtım ile uyumlu segregasyon gösterdi.

DESI1 geni, türler arasında yüksek oranda korunmuş bir sistein proteaz olan PPPDE bölgesi ve nükleer ihracat sinyalleri (NES) içeren bir proteini kodlar. UBQLN ailesi proteinlerinin nükleer çıkışı için adaptör görevi gören DESI1, nükleer taşıma bozukluklarını proteostaz bozukluğuyla bağlayan yeni bir ALS- ilişkili gen adayı olarak karşımıza çıkmaktadır.

Bu varyantların fonksiyonel sonuçlarını araştırmak için, HEK293T hücrelerinde DESI1 varyantlarını aşırı eksprese ettik. Bu deneyler, DESI1 varyantlarının katalitik sistein ve NES gibi kritik bölgelerin eksik olduğu güdük veya anormal proteinlere neden olduğunu gösterdi. Western blot, bu proteinlerin hızla proteazomal yıkıma uğradığını gösterdi. Ko-immunopresipitasyon ise DESI1 ile UBQLN4 arasındaki fiziksel etkileşimin bozulduğunu, ve DESI1'in bilinen substrat BZEL üzerinde deSUMOylaz aktivitesinin kaybolduğunu ortaya koydu. Hasta fibroblastlarında yapılan öncül çalışmalar da proteostaz bozulmasına işaret ederek bu bulguları destekledi.

Bir araya geldiğinde bu bulgular, DESI1'i ALS ile ilişkili yeni bir gen olarak tanımlamakta ve işlev kaybı DESI1 varyantlarının ALS patogenezindeki rolüne dair mekanistik içgörüler sunmaktadır.

ACKNOWLEDGEMENTS

This thesis would not have been possible without the collaboration and collective efforts of many remarkable individuals. To everyone who taught me, guided me, and helped me along this journey. I owe you my deepest gratitude for where I am today.

First and foremost, I would like to express my deepest thanks to Dr. Nathalie Escande Beillard, who has been a guiding light throughout this journey. Her continious support, understanding nature, and unparalleled kindness and care have made all of this possible. I am equally grateful to Dr. Nasrinsadat Nabavizadeh, whose strength and discipline taught me invaluable lessons both in the laboratory and in life. Thanks to Nathalie and Nasrin, I am here today only thanks to them.

I extend my sincere thanks to Dr. Marwan Nashabat for his wisdom and precious advice that guided me through challenging moments. I am also grateful to Burak Sarıbaş and Hilal Pırıl Saraçoğlu for generously sharing their laboratory expertise with me, and to all members of the NEB Lab, Mert, Şeyma and Abdulmalek, with whom I had the privilege of working.

To my esteemed jury members, Dr. Umut Şahin and Dr. Atay Vural, I cannot adequately express my gratitude for your participation in my thesis committee, especially given your extremely busy schedules. Your kindness and understanding in accommodating my extension request, despite your demanding schedules, meant more to me than words can convey.

This research would not have been possible without Prof. Dr. Hülya Kayserili, whose legacy includes building the finest genetics department in Turkey and who is well-respected in the international genetics community, making our current collaborations possible. I am deeply thankful to Dr. Şahin Avcı, who never turned me away whenever I had questions and was always helpful and kind. My gratitude also extends to Dr. Umut Altunoğlu for allowing me to continue this research, and to Prof. Dr. Piraye Oflazer for her collaboration and for sharing the index case with us.

TABLE OF CONTENTS

LIST OF TABLES

LIST OF FIGURES

ABBREVIATIONS

CRM1	Chromosome Region Maintenance 1 (Exportin 1)
DAPI	4′,6-Diamidino-2-Phenylindole
DESI1	DeSUMOylating Isopeptidase 1
DDR	DNA Damage Response
DMEM	Dulbecco's Modified Eagle Medium
DNA	Deoxyribonucleic Acid
dNTP	Deoxynucleotide Triphosphate
DMSO	Dimethyl Sulfoxide
DTT	Dithiothreitol
EtBr	Ethidium Bromide
FBS	Fetal Bovine Serum
GAPDH	Glyceraldehyde 3-Phosphate Dehydrogenase
gDNA	Genomic Deoxyribonucleic Acid
gnomAD	Genome Aggregation Database
HRP	Horseradish Peroxidase
IP	Immunoprecipitation
LB	Luria-Bertani Lysogeny Broth
MCS	Multiple Cloning Site
NES	Nuclear Export Signal
ORF	Open Reading Frame
PCR	Polymerase Chain Reaction
PQC	Protein Quality Control
qPCR	Quantitative Polymerase Chain Reaction
RT-PCR	Reverse Transcription Polymerase Chain Reaction
SDM	Site-Directed Mutagenesis
SENP	Sentrin/SUMO-specific Protease
SUMO	Small Ubiquitin-like Modifier
TBE	Tris-Borate-EDTA Buffer
UPS	Ubiquitin–Proteasome System
WT	Wild Type

Chapter 1:
INTRODUCTION

1.1 Neurodegenerative Diseases

Neurodegenerative diseases are a diverse group of pathologies characterized by progressive and irreversible damage to neurons, leading to their death and thus resulting in neurodegeneration. Neurodegeneration can occur within the central and/or peripheral nervous systems, with different regions of the nervous system being involved depending on the pathomechanism of the disease. Although the involvement of neurodegeneration is quite heterogeneous among diseases, some common pathological features emerge. Some of these hallmarks, which directly or indirectly disrupt the regulation of proteins in the cellular landscape, include cytoskeleton abnormalities, increased inflammatory response, defects in RNA metabolism and regulation, pathological protein aggregation, and disturbances in protein homeostasis (proteostasis) (Wilson *et al.*, 2023).

1.2 Amyotrophic Lateral Sclerosis & Clinical Features

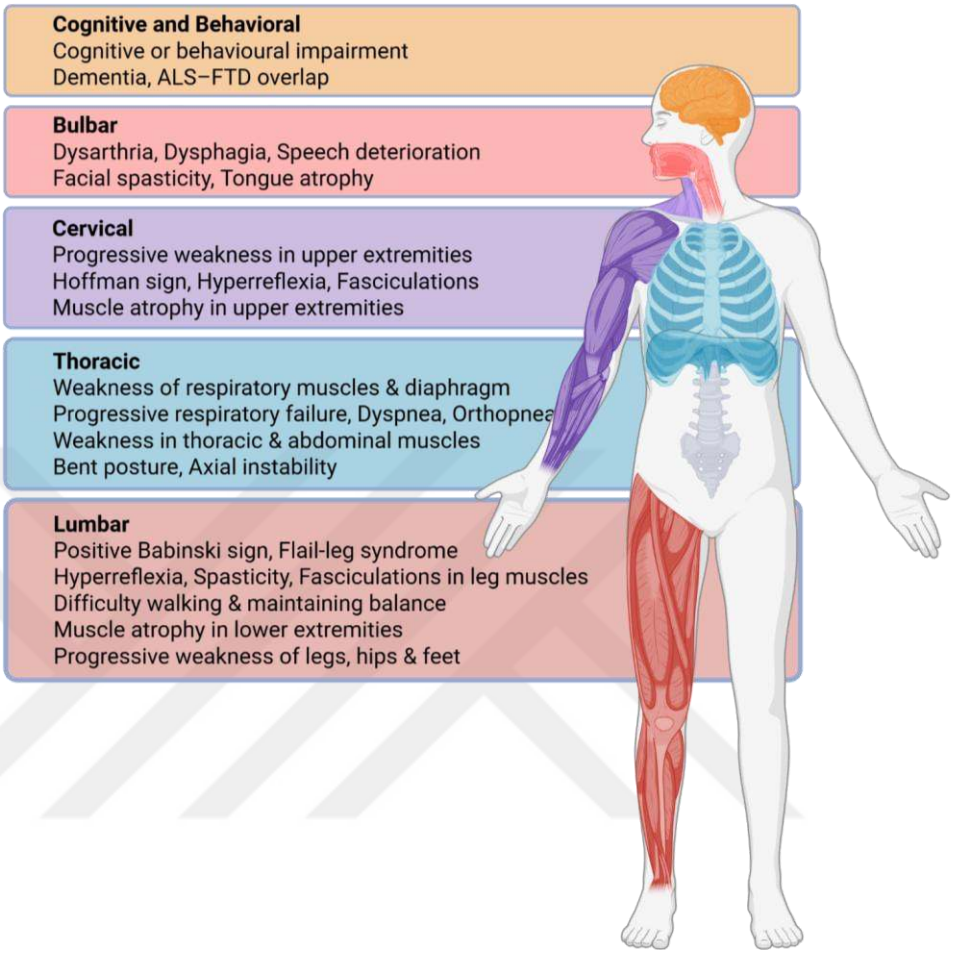

Figure 1.1: Clinical Manifestations and Anatomical Regions Affected in ALS.

Amyotrophic Lateral Sclerosis (ALS) is a progressive neurodegenerative disorder characterized by the degeneration of both upper and lower motor neurons, ultimately leading to neuronal loss and death. Motor neurons innervate skeletal muscles, transmitting signals from the central nervous system to enable voluntary movement. Their degeneration leads to progressive muscular weakness, spasticity, cramps, fasciculations, as well as difficulties in speaking and swallowing (Feldman *et al.*, 2022). ALS is typically a late-onset disease, with an average age of onset around 55 years and a peak incidence at 65 years, however, juvenile-onset forms have also been reported (Hardiman *et al*., 2017; Taylor *et al*., 2016). The disease's symptoms are heterogeneous, ranging from mild to severe. Although the severity and progression of the disease can differ between

individuals, it is invariably fatal. Most patients die from respiratory failure within 3–5 years of the disease onset.

ALS is a rare disease with a prevalence of approximately 0.005% in the general population (Taylor *et al.*, 2016) and is often underdiagnosed or misdiagnosed in its early stages due to clinical overlap with other, more common neuromuscular disorders (Feldman *et al*., 2022).

The etiology of ALS is multifactorial, involving both genetic and environmental contributions. Clinically, the disease is classified into two: Familial ALS (fALS) which accounts for approximately 5–10% of cases, and sporadic ALS (sALS) which represent the remaining (90–95%) of the cases. While sALS patients typically lack a family history of the disease, pathogenic mutations previously identified in fALS are present in sALS as well (Hardiman *et al*., 2017). Approximately 20% of total ALS cases have an identified monogenic cause. A large proportion of these identified genetic mutations are rare, with allele frequencies below 1% in the overall ALS patient population and often follow an autosomal dominant inheritance pattern (Mead *et al.*, 2023). The vast majority, 80% of the cases, lack a molecular diagnosis with approximately 24% of fALS and 75% of sALS cases are not linked to known pathogenic ALS-associated variants (Akçimen *et al.*, 2023).

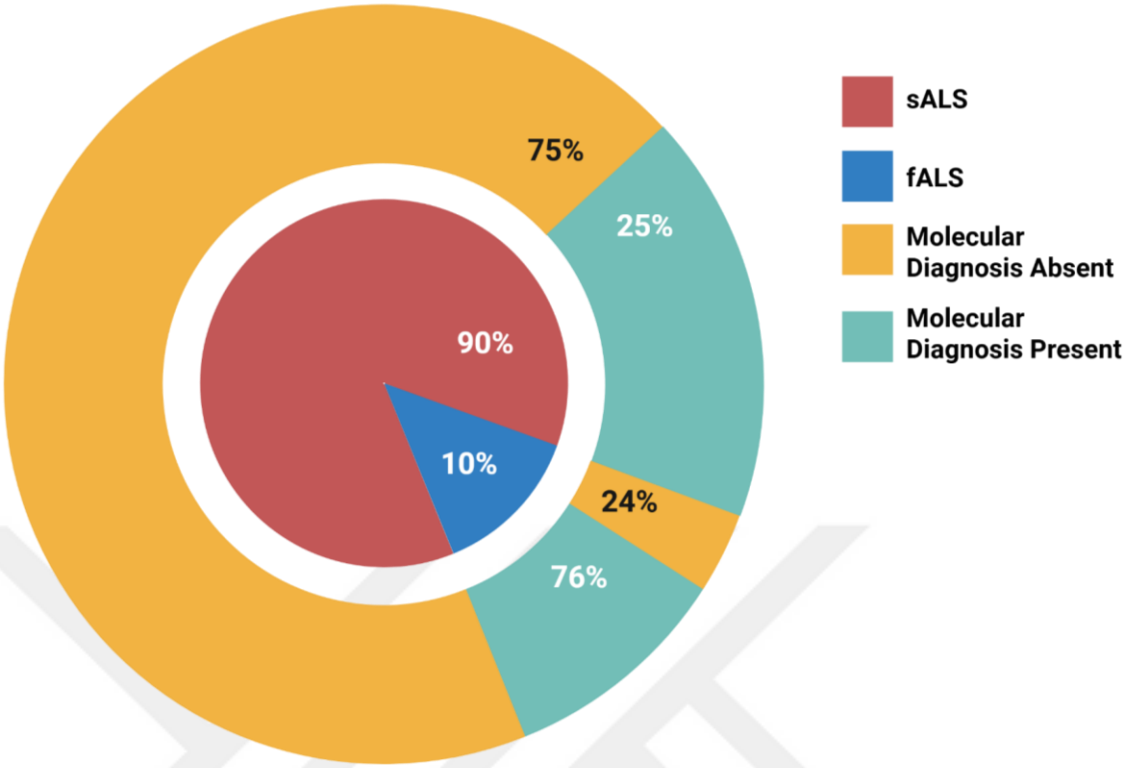

Figure 1.2: Proportions of sALS and fALS Cases Associated with a Molecular Diagnosis.

Similar to many neurodegenerative disorders, the exact pathophysiological mechanisms underlying ALS remain incompletely understood. However, extensive ongoing research aims to improve ALS diagnostic accuracy, deepen our understanding of the disease biology and identify novel therapeutic targets. In particular, genetics studies have been a key player in unraveling disease mechanisms, enabling patient stratification and guiding the development of targeted treatment.

1.3 Genetic and Molecular Pathways Underlying ALS

1.3.1 Genetic Aetiology of ALS

For the first time in 1993, pathogenic variants in a gene, *SOD1*, were identified as the cause of ALS through an investigation of familial ALS cases (Rosen *et al.*, 1993). Since then, pathogenic variants in more than 40 genes have been associated with the disease (Wang *et al.*, 2023), greatly enhancing the diagnosis capabilities and deepening

our knowledge of ALS pathophysiology. Among these, *TARDBP* (MIM: 605078)*, FUS* (MIM: 137070)*, C9orf72* (MIM: 614260)*,* and *SOD1* (MIM: 147450) mutations account for the majority of genetically diagnosed ALS cases. Variants in these genes are found in approximately 60–70% of fALS cases (Mead *et al*., 2023; Hardiman *et al.*, 2017; Taylor *et al*., 2016) and 10–14% of sporadic cases (Akçimen *et al*., 2023; Taylor *et al.*, 2016). Although these four genes represent the most frequent genetic contributors of ALS, numerous rarer genes have also been identified (Table 1.1).

Genes	**MIM**	**Subtype**	**Involved Pathway**	**First Identified**
C9ORF72	614260	FTDALS1	RNA Metabolism and Homeostasis	De Jesus-Hernandez and Renton., 2011
TARDBP	605078	ALS10	RNA Metabolism and Homeostasis	Kabashi *et al*., 2008 Van Deerlin VM *et al*., 2008
FUS	137070	ALS6	RNA Metabolism and Homeostasis	Kwiatkowski and Vance., 2009
ANG	105850	ALS9	RNA Metabolism and Homeostasis	Greenway *et al*., 2006
ATXN2	601517	ALS13	RNA Metabolism and Homeostasis	Elden *et al.*, 2010
HNRNPA1	164017	ALS20	RNA Metabolism and Homeostasis	Kim *et al*., 2013
HNRNPA2B1	600124	MSP/ALS	RNA Metabolism and Homeostasis	Kim *et al*., 2013
MATR3	164015	ALS21	RNA Metabolism and Homeostasis	Johnson *et al*., 2014
TIA1	603518	ALS26	RNA Metabolism and Homeostasis	Mackenzie *et al.*, 2017
CHMP2B	609512	FTDALS7	Protein Quality Control and Proteostasis	Parkinson *et al.*, 2006
OPTN	602432	ALS12	Protein Quality Control and Proteostasis	Maruyama *et al*.,2010

Genes	MIM	Subtype	Involved Pathway	First Identified
VCP	601023	ALS14	Protein Quality Control and Proteostasis/ DNA Damage and Repair	Johnson *et al*., 2010
UBQLN2	300264	ALS15	Protein Quality Control and Proteostasis	Deng *et al*., 2011
SQSTM1	601530	ALS/FTD	Protein Quality Control and Proteostasis	Fecto *et al*., 2011
TBK1	604834	ALS/FTD	Protein Quality Control and Proteostasis, Inflammation	Freischmidt *et al*., 2015
CCNF	600227	FTDALS5	Protein Quality Control and Proteostasis	Williams *et al*., 2016
DNAJC7	601964	ALS	Protein Quality Control and Proteostasis	Farhan *et al.*, 2019
ALS2	606352	ALS2	Cytoskeletal Organization and Axonal Transport	Yang and Hadano., 2001
PFN1	176610	ALS18	Cytoskeletal Organization and Axonal Transport	Wu *et al*., 2012
DCTN1	601143	ALS (HMN7B)	Cytoskeletal Organization and Axonal Transport	Puls *et al.*, 2003
PRPH	170710	ALS (Susceptibility)	Cytoskeletal Organization and Axonal Transport	Corrado *et al.*, 2014
TUBA4A	191110	ALS22	Cytoskeletal Organization and Axonal Transport	Smith *et al.*, 2014
KIF5A	602821	ALS25	Cytoskeletal Organization and Axonal Transport	Nicholas *et al.*, 2018
NEFH	162230	ALS (CMT2CC)	Cytoskeletal Organization and Axonal Transport	Lin *et al.*, 2021
SOD1	147450	ALS1	Oxidative stress and Mitochondrial Function	Rosen *et al*., 1993
VAPB	605704	ALS8	Oxidative stress and Mitochondrial Function	Nishimura *et al*., 2004
SIGMAR1	601978	ALS16	Oxidative stress and Mitochondrial Function	Al-Saif *et al.*, 2011

Genes	MIM	Subtype	Involved Pathway	First Identified
CHCHD10	615903	ALS/FTD	Oxidative stress and Mitochondrial Function	Bannwarth *et al.*, 2014
SPTLC1	605712	ALS27	Lipid Metabolism and Synthesis	Mohassel *et al*., 2021
FIG4	609390	ALS11	Lipid Metabolism and Synthesis	Chow *et al*., 2009
LRP12	618299	ALS28	Lipid Metabolism and Synthesis	Kume *et al.*, 2023
GLT8D1	618399		Lipid Metabolism and Synthesis	Cooper-Knock *et al*., 2019
C21ORF2	603191	ALS	DNA Damage and Repair	van Rheenen *et al.*, 2016
NEK1	604588	ALS24	DNA Damage and Repair	Brenner *et al*., 2016
SETX	608465	ALS4	DNA Damage and Repair	Chen and Moreira., 2004
ERBB4	600543	ALS19	Neuronal Development	Takahashi *et al.*, 2013
ANXA11	*602572*	ALS23	Inflammatory Response	Smith *et al*., 2017

Table 1.1: Key ALS-associated Genes and Their Role in Cellular Pathways

Despite this genetic heterogeneity, many causative genes converge on common cellular pathways underlying motor neuron injury (Table 1.1). These include RNA metabolism and homeostasis as the most represented (nine genes), followed by protein quality control and proteostasis (eight genes), and cytoskeletal organization and axonal transport (eight genes). Additional pathways include mitochondrial function and oxidative stress (four genes), lipid metabolism (four genes), and DNA damage detection and repair (three genes) (Fig 1.3). Understanding how ALS-associated pathogenic variants disrupt these pathways is essential for elucidating disease mechanisms and identifying therapeutic targets. Nevertheless, despite major advances in gene discovery, the majority of ALS patients still lack a molecular diagnosis, highlighting the need for continued exploration of the genetic and molecular basis of this disease.

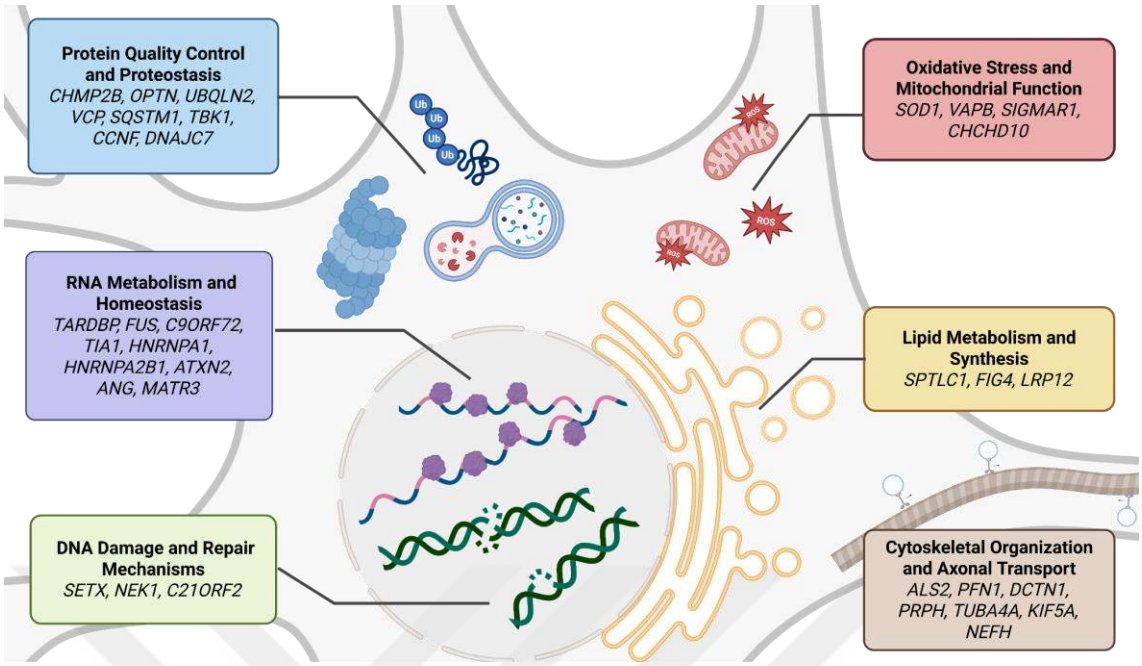

Figure 1.3: ALS-Associated Genes and Their Involved Pathways.

1.3.2 RNA Metabolism and Homeostasis

Two interconnected mechanisms, disturbances in proteostasis and defects in RNA metabolism, have emerged as key features of ALS pathology. Consistent with this, a substantial proportion (16/44) of ALS-linked mutations occur in genes directly involved in these pathways or result in their disruption (Table 1.1 and Figure 1.3).

Disturbances in RNA processing are major drivers of ALS pathogenesis. TDP-43, encoded by the *TARDBP* gene, is a DNA/RNA-binding protein primarily localized in the nucleus but capable of shuttling between the nucleus and cytoplasm (Ayala *et al.,* 2008). It plays key roles in RNA splicing, transcriptional regulation, and stress granule formation (Ling *et al.*, 2013). However, in ALS, TDP-43 mislocalizes to the cytoplasm where it forms pathological aggregates. Cytoplasmic TDP-43 inclusions are a major hallmark of ALS present in 97% of ALS cases, even in the absence of *TARDBP* mutations (Hardiman *et al*., 2017; McAlary *et al*., 2020; Mead *et al*., 2023). Similarly, the FUS protein, produced by *FUS*, is another RNA-binding protein involved in RNA splicing, transcription regulation, and stress granule formation (Ling *et al.*, 2013). Like TDP-43, FUS undergoes pathological mislocalization and forms cytoplasmic inclusions in ALS (Deng *et al.*, 2010). In both cases, the mislocalization and the absence of functional

protein result in a loss of normal nuclear function, while protein aggregation in the cytoplasm leads to cellular toxicity.

Heterogeneous nuclear ribonucleoproteins (hnRNPs) A1 and A2B1 have also been implicated in ALS and multisystem proteinopathy (Kim *et al.*, 2013). These hnRNPs share notable functional and structural homology with TDP-43 and FUS, characterized by low-complexity domains (LCDs) that enable their functions in RNA metabolism and phase separation. While LCDs are crucial for normal protein function, they also confer susceptibility to pathological aggregation (Kim *et al.*, 2013; Harrison & Shorter, 2017). Although less investigated than the previous, *MATR3* encodes Matrin-3, a DNA/RNA binding protein that interacts with TDP-43 and was identified in a large fALS cohort (Johnson *et al*., 2014). Meanwhile, expansions of 6-nucleotide repeat in C9orf72 result in accumulation and aggregation of toxic dipeptides that can impair critical cellular functions such as RNA metabolism and intracellular trafficking (Cooper-Knock *et al*., 2014; Zhang *et al*., 2015).

1.3.3 Cytoskeletal Organization and Axonal Transport

Neurons rely on their specialized morphology to perform their functions, requiring both cytoskeletal integrity and efficient biomolecule transport to maintain activity and survival (Theunissen *et al.*, 2021). Axonal transport is essential for neuronal homeostasis allowing proper localization through bidirectional processes. Anterograde transport delivers newly synthesized biomolecules and organelles to required axonal sites, while retrograde transport returns damaged components for degradation and recycling (Theunissen *et al.*, 2021). Pathogenic variants identified in genes encoding motor proteins and cytoskeletal elements such as *DCTN1* (Puls *et al.*, 2003), *PRPH* (Corrado *et al.*, 2011), *TUBA4A* (Smith *et al.*, 2014), *KIF5A* (Nicholas *et al.*, 2018), and *NEFH* (Lin *et al.*, 2021) have been associated with ALS (Figure 1.3). These variants disrupt cytoskeleton integrity and axonal transport, thereby compromising motor neuron viability.

Additional mechanism contributing to cytoskeletal impairment involves inclusions containing neuron-specific intermediate filaments, which are thought to result from TDP-43 aggregation in ALS (Atkinson *et al.,* 2021).

1.3.3 Oxidative stress and Mitochondrial Function

Oxidative stress and mitochondrial dysfunction represent key pathological features of ALS (Figure 1.3). Reduced glutathione (GSH) levels have been observed in ALS patients' nervous systems (ALSuntangled group, 2019), while increased cellular oxidation contributes to damage of DNA, RNA, lipids, and proteins (Hemerkova and Valis, 2021). This oxidative damage also impairs mitochondrial function and decreases ATP synthesis through several mechanisms (Guo *et al.*, 2013), including disruption of Ca2+ homeostasis (Barsukova *et al.*, 2011) and oxidative phosphorylation (Singh *et al,* 2019). Furthermore, increased oxidative stress promotes aggregation of ALS-linked proteins such as SOD1 and TDP-43 (Carri *et al.*, 2015).

The *SOD1* gene, encoding superoxide dismutase 1—a key antioxidant enzyme, was the first identified ALS gene (Rosen *et al.*, 1993) and remains one of the most studied. In SOD1 mutant ALS mouse models, progressive GSH depletion and increased spinal oxidative stress have been observed (Chi *et al.*, 2007). Additionally, SOD1 inclusions can accumulate on mitochondrial membranes, disrupting mitochondrial transport (Tafuri *et al*., 2015) or triggering apoptosis via cytochrome-c release (Pedrini *et al*., 2010).

Several other ALS causative genes are directly linked to oxidative stress regulation and mitochondrial function. CHCHD10, a mitochondrial protein involved in cristae stability, has been associated with both ALS and FTD (Bannwarth *et al.*, 2014). VAPB, a protein residing in ER-mitochondrial contact sites, has been linked to ALS (Nishimura *et al*., 2004) and functions in maintaining Ca^{2+} homeostasis via interaction with PTPIP51; a complex disrupted in TDP-43 pathology (Stoica *et al*., 2014). Similarly, *SIGMAR1*, encoding another protein present in ER-mitochondrial contact sites, has been associated with ALS with dementia (Belzil *et al.*, 2012). Increased oxidative stress may exacerbate excitotoxicity in ALS through upregulation of the cysteine/glutamate antiporter in glial cells (Provenzano *et al*., 2023).

1.3.4 DNA Damage and Repair Mechanisms

Neurons are terminally differentiated, post-mitotic cells that can no longer dilute DNA lesions through cell division. As a result, they are particularly vulnerable to the accumulation of DNA damage, especially with aging, and rely on DNA damage response and repair (DDR) mechanisms to maintain genomic integrity. R-loops and G-quadruplex

structures occurring during physiological events such as transcription make the genome susceptible to DNA damage. *SETX*, encoding the senataxin protein, is among the first genes linked to ALS, and identified as the causative gene for juvenile-onset ALS4 (Chance *et al*., 1998; Chen *et al*., 2004). Senataxin is an RNA/DNA helicase, playing a role in DDR by resolving R-loops and is actively recruited to sites of DNA damage (Kannan *et al*., 2022).

Other ALS-associated components, NEK1 and C21ORF2, are also involved in DDR. These two proteins cooperate by binding and stabilizing each other. NEK1, a serine/threonine kinase participating in DDR signaling, is known to phosphorylate downstream effectors. Meanwhile, C21ORF2 binds and protects NEK1 from degradation to ensure proper repair activity (Fang *et al*., 2015). An ALS-linked variant in C21ORF2 (V58L) leads to NEK1 downregulation and consequent DNA damage accumulation in iPSC-derived motor neurons (Zelina *et al.*, 2024).

1.3.6. Lipid Synthesis and Metabolism

Emerging evidence implicates dysregulated lipid metabolism and synthesis as a pathological feature of ALS. Lipids serve as structural components of cellular membranes, signaling molecules, and energy sources through mitochondrial β-oxidation. Several ALS-associated genetic variants directly affect lipid pathways: mutations in *SPTLC1*, encoding a subunit of serine palmitoyl transferase responsible for de novo sphingolipid synthesis, cause childhood-onset ALS (Mohassel *et al*., 2021). Additionally, pathogenic variants in *FIG4*, a phosphoinositide 5-phosphatase regulating the signaling molecule $PI(3,5)P_2$ levels and therefore retrograde transport, are present in approximately 2% of ALS/PLS patients (Chow *et al*., 2009). Repeat expansions in *LRP12*, encoding an LDL receptor-related protein involved in signal transduction, have also been identified in ALS cases (Kume *et al*., 2023).

1.3.7. Protein Quality Control and Proteostasis

Protein aggregation, a hallmark of ALS pathology, reflects proteostatic failure in ALS pathogenesis. Defective protein quality control systems, including the ubiquitin–proteasome system (UPS) and autophagy–lysosome pathway lead to the accumulation of

toxic aggregates that sequester cellular components and promote motor neuron degeneration.

Likewise, mutations in the *SOD1* gene lead to protein misfolding and the formation of toxic cytoplasmic inclusions that impair critical cellular functions (Akçimen *et al.*, 2023). Additionally, mutant SOD1 impairs the clearance of misfolded proteins by inhibiting endoplasmic reticulum–associated degradation (ERAD), a key proteostatic pathway (Taylor *et al.*, 2016).

Since the discovery of *SOD1,* numerous genes encoding proteins with direct roles in autophagy or the UPS have been implicated in ALS, including *VAPB* (Nishimura *et al.*, 2004), *CHMP2B* (Parkinson *et al.*, 2006), *VCP* (Johnson *et al.*, 2010), *OPTN* (Maruyama *et al.*, 2010), *SQSTM1 (p62)* (Fecto *et al.*, 2011), *UBQLN2* (Deng *et al.*, 2011), and *TBK1* (Freischmidt *et al.*, 2015). Together, these findings establish pathogenic variants in PQC and proteostasis pathways representing the second largest group of ALS-associated genes. Mutations in these genes can perturb proteostasis through multiple mechanisms. TBK1, by phosphorylating the autophagy receptors SQSTM1/p62 (Matsumoto *et al.*, 2015) and OPTN (Richter *et al.*, 2016), is involved in the initiation of autophagy. Phosphorylation of these receptors allows them to bind ubiquitinated cargo and LC3, which is essential for autophagosomal engulfment (Parzych and Klionsky, 2014). Collectively, these discoveries underline that defects in proteostasis, quality control and clearance play a pivotal role in ALS pathology (Ling *et al*., 2013).

1.4 UBQLNs in Proteostasis and ALS

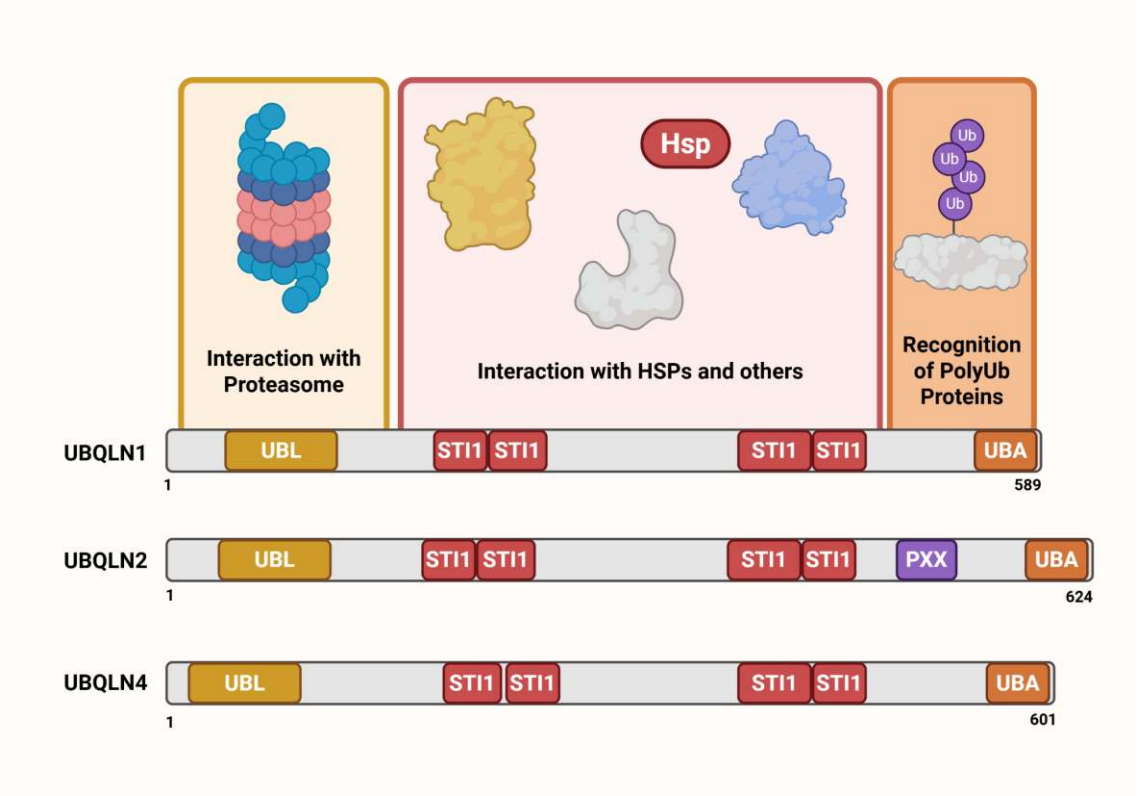

Figure 1.4: Domain Architecture and Functional Interactions of UBQLN Family Proteins. UBL: Ubiquitin-like domain, STI1: Stress-inducible protein 1 homology domain, PXX: Proline-rich region, UBA: Ubiquitin-associated domain

A highly conserved protein family in mammals, the ubiquilins (UBQLNs), orchestrate the recognition and transport of polyubiquitinated proteins to proteasome. UBQLNs serve as key proteostasis regulators, linking the UPS and autophagy pathways while participating in cellular stress responses (Lin *et al*., 2022; Marin, 2014; Zheng *et al.*, 2020). Five UBQLN genes have been identified in humans: UBQLN1, UBQLN2, and UBQLN4 are expressed in multiple tissues including the brain, whereas UBQLN3 and UBQLNL show testis-specific expression (Gerson *et al*., 2021; Lin *et al*., 2021; Human Protein Atlas). UBQLN proteins share a conserved architecture with an N-terminal ubiquitin-like (UBL) domain that binds to the proteasome, a C-terminal ubiquitin-associated (UBA) domain that recognizes the ubiquitinated substrates, and STI1 domains that interact with molecular chaperones such as Hsp70 (Hjerpe *et al*., 2016) (Figure 1.4). This structure enables the UBQLNs to function as molecular shuttles that deliver

misfolded proteins for degradation. Therefore, the functionality of UBQLNs holds potential significance in understanding ALS pathogenesis.

Among the family members, UBQLN2 shows the strongest association with ALS. Since its first identification in X-linked ALS by Deng *et al*. (2011), multiple pathogenic *UBQLN2* variants have since been discovered (Deng *et al*., 2011; Synofzik *et al*., 2012), establishing *UBQLN2* as a well-known ALS causative gene. Most ALS-associated pathogenic variants of *UBQLN2* cluster within the proline-rich domain and impair proteasomal degradation (Deng *et al*., 2011). UBQLN2 can directly bind to the C-terminus of TDP-43 and, as an essential part of UPS, mediates degradation of full-length and C-terminal fragments of TDP-43 found in ALS patients (Suk *et al*., 2020). While the loss of UBQLN2 function impairs the clearance of pathological aggregates of TDP-43 as well as FUS (Hjerpe *et al*., 2016), conversely, both the ALS-associated mutant and the wild-type UBQLN2 can alter TDP-43's subcellular localization and promote cytoplasmic inclusions (Renaud *et al*., 2019). Strikingly, wild-type UBQLN2 is found in pathological inclusions in sporadic ALS cases, suggesting that UBQLN2 dysfunction extends beyond genetic variants.

UBQLN4, encoding UBQLN4, has also been linked to ALS, although only a single pathogenic variant (D90A) has been reported in familial cases to date (Edens *et al*., 2017). This variant is located near the UBL domain. Beyond proteostasis, UBQLN4 also participates in the DNA damage response (DDR), where it is phosphorylated by ATM and translocates to the nucleus to influence pathway choice by regulating the turnover of DDR-associated proteins (Jachimowicz *et al*., 2019).

Although *UBQLN1* is not directly implicated in ALS, a pathogenic variant (E54D) in the UBQLN1 protein has been reported in Brown-Vialetto-Van Laere (BVVL) syndrome, a motor neuron disorder characterized by sensorineural hearing loss. Despite not being directly implicated in ALS, UBQLN1 influences TDP-43 pathology and proteostasis, with expression levels correlating with disease progression (González-Pérez *et al*., 2012; Yu *et al*., 2024).

A functional interplay between UBQLNs is also evident. While UBQLN4 can act as an adaptor for UBQLN1 recruitment to autophagosomes (Şentürk *et al*., 2019), UBQLN1

overexpression may be compensatory for *UBQLN2* pathogenic variants, as it was found to reduce aggregates and restore proteostasis in UBQLN2 mutant mice (Wang *et al.*, 2020).

1.5 Desumoylating Isopeptidase 1: a shared interactor of UBQLNs

Desumoylating Isopeptidase 1 (*DESI1*) gene (also referred as POST or PPPDE2), is located on chromosome 22 and composed of six exons, encoding a small protein of 168 amino acids (20 kDa). The human DESI1 protein is highly conserved across species (Figure 1.5).

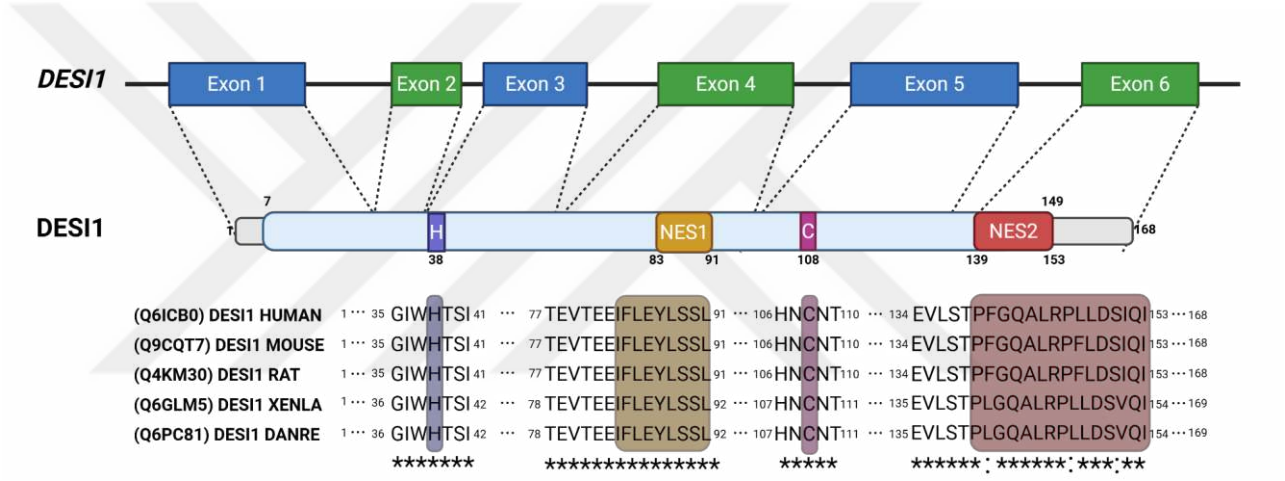

Figure 1.5: Gene Structure, Protein Domain Organization, and Evolutionary Domain Conservation Across Species.

DESI1 contains a 143 amino acid-long Permuted Papain fold Peptidases of Ds-RNA viruses and Eukaryote (PPPDE) domain that mediates its deSUMOylase activity, hence its name "deSUMOylating Isopeptidase 1". This catalytic domain contains a strictly conserved histidine (His38)-cysteine (Cys108) dyad positioned within 3.1 Å in the folded protein structure (Suh *et al.*, 2012). DESI1 functions as a homodimer, with these catalytic residues forming the core of its active site groove (Suh *et al.*, 2012). Currently, the transcription factor BZEL (ZBTB46) remains the only identified and experimentally validated substrate of DESI1 deSUMOylase activity (Shin *et al.*, 2012) (Figure 1.6). In addition to its deSUMOylase activity, PPPDE domain of DESI1 shows dual enzymatic activity by displaying palmitoyl protein thioesterase function, enabling S-

depalmitoylation of substrate proteins (Luebben *et al*., 2022), however no physiological substrates have been identified to date.

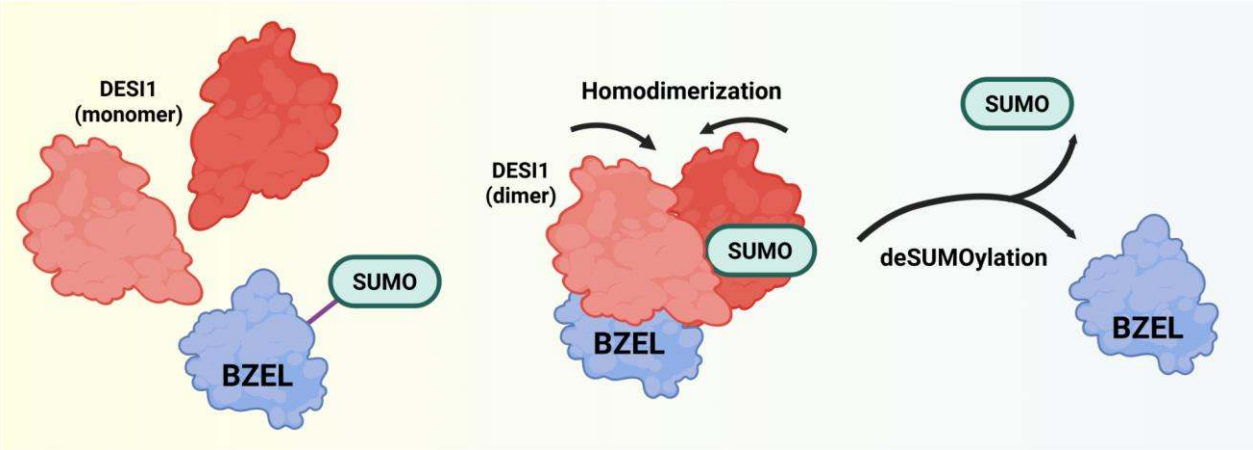

Figure 1.6: DeSUMOylation activity of DESI1.

DESI1 also plays a critical role in the Nuclear Transport System. The protein possesses two intrinsic NES sequences (NES1: reverse-type NES and NES2: canonical NES) near the C-terminus. Through NES2, DESI1 interacts with the general nuclear export receptor Exportin-1 (XPO1 / CRM1) (Hirayama *et al.*, 2018). Importantly, DESI1 partners with UBQLN4, acting as a nuclear export adaptor for this brain-expressed UBQLN (Hirayama *et al.*, 2018). Mass spectrometry data further revealed that DESI1 also interacts with UBQLN1 and UBQLN2, other abundantly brain-expressed UBQLN, (Hirayama *et al.*, 2018). Since UBQLNs lack intrinsic NES sequences, they cannot be exported from the nucleus independently. By partnering with DESI1, UBQLNs are transported from the nucleus to the cytoplasm, allowing the translocation of polyubiquitinated proteins including those targeted for proteasomal degradation (Hirayama *et al.*, 2018) (Figure 1.7).

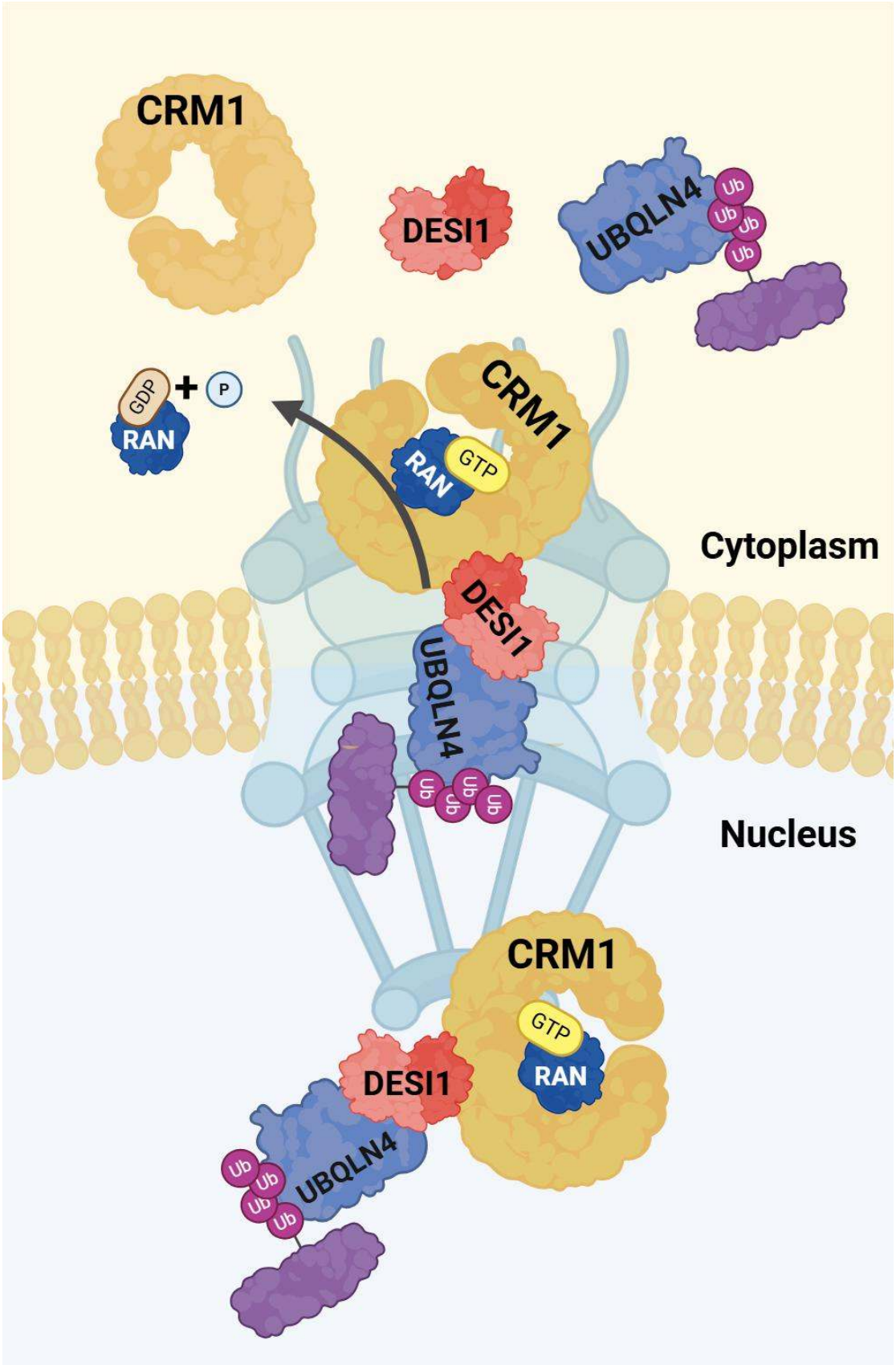

Figure 1.7: CRM1 Mediated Nuclear Export of DESI1 and UBQLN4.

Currently, no cellular or animal models demonstrating loss-of-function or gain-of-function in DESI1 have been reported. Additionally, no pathogenic variants in the *DESI1* gene have been identified in human diseases through genetic studies or clinical case reports. Although enzymatic functions and structural characteristics of DESI1 have been characterized, the lack of functional models and disease-associated variants represents a critical gap in our understanding of its physiological roles and potential involvement in neurodegeneration.

Chapter 2:
MATERIALS AND METHODS

2.1 RNA and DNA Isolations and cDNA Synthesis

2.1.1 RNA Isolation

RNA isolation from primary patient fibroblasts and cell lines was performed using the RNeasy Mini Kit (Qiagen, Cat#74104). Approximately 5 $\times 10^6$ cells were used for RNA extraction from HEK293T and SH-SY5Y cell lines, whereas 6 $\times 10^5$ primary patient fibroblasts were used. RNA extraction was performed according to the manufacturer's protocol, and on-column DNase treatment was performed. RNA concentrations were measured using a NanoDrop™ 2000c (Thermo Scientific, Cat#ND-2000C) and stored at -80ºC in an ultra-freezer until use.

2.1.2 cDNA Synthesis

cDNA synthesis from RNA extractions was performed using two different kits: the iScript Reverse Transcriptase Kit (Bio-Rad, Cat#1708891) and LunaScript RT SuperMix Kit (NEB, Cat#E3010L). 1000 ng of RNA extracted was used for cDNA synthesis. The reaction mixes and thermal cycling conditions are listed below.

Component	**Volume**
5X Reaction Mix	4 µl
iScript Reverse Transcriptase	1 µl
RNA Template	x µl (1000 ng)
ddH2O	up to 20 µl

Table 2.1: iScript Reverse Transcriptase Reaction

Step	Temperature	Duration
1	25ºC	5:00
2	46ºC	20:00
3	95ºC	1:00
4	4ºC	Hold

Table 2.2: iScript Reverse Transcriptase Thermal Cycling Conditions

Component	Volume
5X Reaction Mix	4 µl
RNA Template	x µl (1000 ng)
ddH2O	up to 20 µl

Table 2.3: LunaScript RT Supermix Reaction

Step	Temperature	Duration
1	25ºC	2:00
2	46ºC	10:00
3	95ºC	1:00
4	4ºC	Hold

Table 2.4: LunaScript RT Supermix Thermal Cycling Conditions

2.1.3 RT-PCR

Target sequences were amplified from synthesized cDNA using Q5 High-Fidelity DNA Polymerase (NEB, Cat#M0491L). Thermal cycling was performed using Veriti 96-Well Fast Thermal Cycler (Applied Biosystems, Cat#4375305). Annealing temperatures for primer pairs were calculated using the NEB Tm Calculator specifically optimized for Q5 High-Fidelity DNA Polymerase (https://tmcalculator.neb.com/#!/main).

PCR products were analyzed by agarose gel electrophoresis using 1.2% agarose gel containing EtBr. The reaction master mix (Table 2.5) thermal cycling conditions (Table 2.6) are presented below.

Component	**Volume**
5x Reaction Buffer	5 µL
Q5 High-Fidelity DNA Polymerase	0.25 µL
dNTP (10 mM)	0.5 µL
Forward primer (10 µM)	1.25 µL
Reverse primer (10 µM)	1.25 µL
cDNA template	X µL (1000 ng)
ddH2O	to 25 µL

Table 2.5: Q5 HF DNA Polymerase Master Mix for cDNA Templates

Step	**Temperature**	**Duration**	**Cycle**
1	98°C	0:30	1
2	98°C	0:10	35
	Variable	0:30	
	72°C	Variable (30sec/kb)	
3	72°C	2:00	1
4	4°C	Hold	1

Table 2.6: RT-PCR Thermal Cycler Program

2.1.4 RT-quantitative PCR (RT-qPCR)

RT-qPCR was performed using cDNA synthesized as described in section 2.1.2. Reactions were performed on PikoReal 96 Real-Time PCR System (Thermo Scientific, Cat#N11471). LightCycler 480 SYBR Green I Master (Roche, Cat#04707516001) was

used as a master mix for amplification and fluorescent dye. GAPDH was used as a reference gene for normalization. Details for master mix and cycling conditions are provided in Table 2.7 and Table 2.8.

Component	**Volume**
LightCycler 480 SYBR Green I Master	5 µL
Primer Mix	0.1 µL
ddH20	3.9 µL
cDNA template	1 µL

Table 2.7: RT-qPCR Reaction Mix

Step	**Temperature**	**Duration**	**Cycle**
1	95°C	7:00	1
2	95°C	0:05	40
	53°C	0:30	
3	53°C	0:30	1
Melt Curve	53-95°C		1

Table 2.8: qPCR Cycling Conditions

2.1.5 Genomic DNA Isolation

Genomic DNA (gDNA) was isolated from primary fibroblasts of patients and wild-type (WT) controls using approximately 1×10^6 cells suspended in 200 µL PBS. The Quick-DNA Miniprep Plus Kit (Zymo Research, Cat#D4069) was used for isolation. Proteinase K digestion at 55 °C was performed using the Biofluid & Cell Buffer from the kit. All steps were performed according to the established protocol. Purified gDNA samples were eluted in a 50 µl volume. Sample concentrations were measured using a NanoDrop™ 2000c and stored at -20 °C until use.

2.2 Generation of Overexpression Constructs

2.2.1 Designing Cloning Primers

Cloning primers were designed to target the open reading frames (ORF) of the genes of interest. Primer length, GC content, and melting temperature optimization were calculated based on the gene-specific sequences of the primers. All were optimized according to the recommendations for efficient and specific amplification. Epitope tags were introduced into the forward primers for N-terminal tagging and reverse primers for C-terminal tagging. In addition, a Kozak sequence (GCCACC) was integrated into the primer to enhance protein translation during the overexpression process. Finally, a restriction enzyme recognition site was included in the primer sequence to enable digestion of the product and ligation with the vector. Depending on the restriction enzyme, 2-8 nucleotides were included in the primer sequence before the restriction enzyme site to enhance the digestion reaction. The primer design strategy is schematically represented in Figure 2.1 and all cloning primer sequences are listed in Table 2.9.

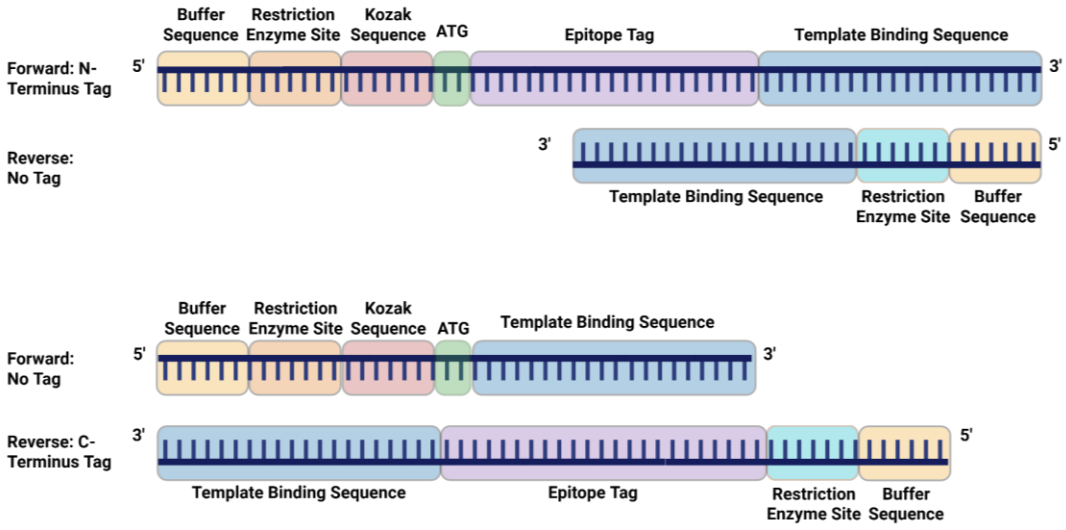

Figure 2.1: Design Strategy for Cloning Primers.

Primer Name	Strand	Primer Sequence	Target
MYC-DESI1-F	F	ACGTACGTGGATCCGCCACCATGGAGC AAAAGCTCATTTCTGAAGAGGACTTGG AGCCGCCGAATCTCTAT	DESI1 ORF
FLAG-DESI1-F	F	ACGTACGTGGATCCGCCACCATGGATT ACAAGGATGACGACGATAAGCATATGG AGCCGCCGAATCTCTAT	DESI1 ORF
HA-DESI1-F	F	ACGTACGTGGATCCGCCACCATGTACC CATACGACGTCCCAGACTACGCTATGG AGCCGCCGAATCTCTAT	DESI1 ORF
DESI1-R	R	GCAACTCGAGTTAGCTCTGGCCGTTGG	DESI1 ORF
FLAG-UBQLN2-F	F	ACGTACGTGGATCCGCCACCATGGATT ACAAGGATGACGACGATAAGGCTGAG AATGGCGAGAGCAG	DESI1 ORF
UBQLN2-R	R	GCAACTCGAGTTACGATGGCTGGGAGC C	DESI1 ORF
MYC-BZEL-F	F	ACGTACGTGGATCCGCCACCATGGAGC AAAAGCTCATTTCTGAAGAGGACTTGA ACAACCGAAAGGAAGATATGG	BZEL ORF
BZEL-R	R	GCAACTCGAGCTAGGAGAGCCAGGCG AAG	BZEL ORF
HA-SUMO1-F	F	ACGTACGTGGATCCGCCACCATGTACC CATACGACGTCCCAGACTACGCTTCTG ACCAGGAGGCAAAAC	SUMO1 ORF
SUMO1-R	R	GCAACTCGAGCTAAACTGTTGAATGAC CCCC	SUMO1 ORF
HA-SUMO2-F	F	ACGTACGTGGATCCGCCACCATGTACC CATACGACGTCCCAGACTACGCTGCCG ACGAAAAGCCCAA	SUMO2 ORF
SUMO2-R	R	GCAACTCGAGTCAGTAGACACCTCCCG TCTGC	SUMO2 ORF
HA-SUMO3-F	F	ACGTACGTGGATCCGCCACCATGTACC CATACGACGTCCCAGACTACGCTTCCG AGGAGAAGCCCAAG	SUMO3 ORF

SUMO3-R	R	GCAACTCGAGCTAGAAACTGTGCCCTG CCA	SUMO3 ORF

Table 2.9: Cloning Primers' Sequences

2.2.2 Insert Amplifications

2.2.2.1. DESI1 WT and Mutant ORF Insert Amplification

The ORF of the WT *DESI1* Gene was amplified from the HA-tagged WT-DESI1 ORF construct kindly gifted by Dr. Hirayama (University of Tokyo, Japan). Primers targeting the complete ORF were used for amplification. The design of the primers is explained in Section 2.2.1. MYC or FLAG epitope tags and BamHI restriction enzyme sites were introduced to the N-terminus, and XhoI restriction enzyme sites were introduced to the C-terminus using primers during amplification. For the patient F1:II.2, carrying the variant *v*1 (c.413+1 G>A), cDNA from patient-derived fibroblasts was used as a template, which showed exon 5 skipping. Q5 High-Fidelity DNA Polymerase (NEB, Cat#M0491L) was used to amplify the inserts. PCR products were visualized by agarose gel electrophoresis using a 1.2% agarose gel prepared with ethidium bromide (EtBr) and 0.5% TBE Buffer. A 1 kb (Thermo Scientific, Cat#SM0311) and a 100 bp DNA ladder (Thermo Scientific, Cat#SM0241) were used to identify the corresponding DNA bands, which were excised from the gel using clean scalpels to prevent contamination and extracted from gel pieces using the NucleoSpin PCR and Gel Clean Up Kit (Macherey-Nagel, Ref#740609.50). Extraction was performed according to the manufacturer's protocol.

2.2.2.2 UBQLN1 and UBQLN2 Cloning Insert Amplification

Constructs containing Flag-tagged UBQLN1 and UBQLN2 in the pCMV4+ backbone were kindly provided by Dr. Ivanova (University of Michigan, USA). The gifted construct for UBQLN1 had intact restriction enzyme sites for BamHI and XhoI. 1000 ng of pCMV4+-N-Flag-UBQLN1 was digested using 10U BamHI-HF (NEB, Cat# R3136S) and 10U XhoI (NEB, Cat#R0146S) enzyme for 1 hour at 37ºC. DNA bands from the digestion reaction were visualized by agarose gel electrophoresis using a 1.2% agarose gel prepared with EtBr and 0.5% TBE Buffer. A 1 kb DNA ladder was used to

identify the DNA bands. The DNA band at approximately 1800 bp was excised with a clean scalpel, and DNA extraction from the gel was performed using the NucleoSpin PCR and Gel Clean Up Kit. The original pCMV4+-N-Flag-UBQLN2 construct had been prepared using XbaI and HindIII restriction enzymes; however, the site for XbaI recognition lost its uniqueness during the process and needed to be re-cloned by PCR amplification. The design of the primers is explained in the related section. Q5 High-Fidelity DNA Polymerase (NEB, Cat#M0491L) was used to amplify the N-Flag-UBQLN2 insert.

2.2.2.3 SUMO1, SUMO2, SUMO3 and BZEL Insert Amplification

The design of cloning primers for *SUMO1*, *SUMO2*, *SUMO3*, and *BZEL* are explained in the related section. cDNA from the human cell line HEK293T was used to amplify inserts for *SUMO1*, *SUMO2*, and *SUMO3*, as these genes are ubiquitously expressed. N-terminal HA-tag and restriction sites for BamHI and XhoI were introduced using primers. Due to the tissue-specific expression of *BZEL*, cDNA from the human neuroblastoma cell line SH-SY5Y was used. Restriction enzyme sites BamHI and XhoI and an N-terminal MYC-Tag were introduced using primers. Q5 High-Fidelity DNA Polymerase was used for the amplification of the inserts from cDNA templates.

2.2.2.4 Site-Directed Mutagenesis

For those variants we don't have access to the patient samples (v3: c.289C>T; v4: c.417delC), site-directed mutagenesis (SDM) was performed to replicate patient-specific mutations in WT constructs. The QuikChange II XL Site-Directed Mutagenesis kit (Agilent Technologies, Cat#200522) was used. Mutagenic primers were designed following the manufacturer's recommendations and Agilent's online mutagenic primer design tool at https://www.agilent.com/store/primerDesignProgram.jsp address. All primers were 25-45 bp in length with melting temperatures (Tm) above 78°C, and the desired mutation was located near the center of the primer. Primer sequences for SDM can be found in table 2.10. For the mutagenesis reaction, 50 ng of plasmid DNA template was used. Reaction mixes and thermal cycling conditions for the reaction are given in Table 2.11 and Table 2.12.

Primer Name	Strand	Primer Sequence	Target
DESI1 c.322dup SDM F	F	CCTACAACCTCTTTGAACACAATTTGTAACACCTTCAGC	*DESI1 v2*
DESI1 c.322dup SDM R	R	GCTGAAGGTGTTACAAATTGTGTTCAAAGAGGTTGTAGG	*DESI1 v2*
DESI1 c.289C>T SDM F	F	GTAGGCCTCACCTCAGAACAGGGACTCCC	*DESI1 v3*
DESI1 c.289C>T SDM R	R	GGGAGTCCCTGTTCTGAGGTGAGGCCTAC	*DESI1 v3*
DESI1 c.417delC SDM F	F	GAAGTGCCTGTCCAAAGGCGTGGAGAGAACTT	*DESI1 v4*
DESI1 c.417delC SDM R	R	AAGTTCTCTCCACGCCTTTGGACAGGCACTTC	*DESI1 v4*
DESI1 c.290+2T>A SDM F	F	GTCCCTGTTCCGGAGAGTGGAGACAGG	*DESI1 v5*
DESI1 c.290+2T>A SDM R	R	CCTGTCTCCACTCTCCGGAACAGGGAC	*DESI1 v5*
DESI1 c.291-4A>G SDM F	F	TGCAAACCTTTCAATGTGCAGAGGTGAGGCCTACA	*DESI1 v6*
DESI1 c.291-4A>G SDM R	R	TGTAGGCCTCACCTCTGCACATTGAAAGGTTTGCA	*DESI1 v6*

Table 2.10: Primer Sequences for SDM

Component	Volume
10X Reaction Buffer	5 µL
Template DNA	x µL (50 ng)
F Primer	x µL (125 ng)
R Primer	x µL (125 ng)
dNTP	1 µL
Quik Solution	3 µL
ddH20	to 50 µL
PFU Turbo DNA Polymerase	1 ul

Table 2.11: SDM PCR Reaction Mix

Step	Temperature (°C)	Duration	Cycle
1	95	1:00	1
2	95	0:50	18
	60	0:50	
	68	5:00	
3	68	7:00	1
4	4	Hold	1

Table 2.12: SDM Thermocycler Protocol

After PCR amplification, DpnI enzyme was used to remove methylated parental strands from the reaction. 10 U of DpnI was mixed with the PCR product and incubated at 37°C for 1 hour, according to the kit's protocol.

2.2.3 Cloning into Mammalian Expression Vectors

The empty pCS2+ vector modified with a T7 promoter downstream of the multiple cloning site (MCS) was used as a backbone for transient overexpression in mammalian cell cultures for each gene of interest. Meanwhile, the empty pCDNA3.1+ vector was used to create stable overexpression constructs only for N-MYC-DESI1 WT, N-MYC-DESI1 c.413+1G>A, and N-MYC-DESI1c.322dupT inserts.

Restriction enzyme sites BamHI and XhoI in the MCS of both plasmids were digested overnight at 37ºC using BamHI-HF and XhoI restriction enzymes to create DNA overhangs. The empty backbone (1000 ng) was digested using 10U BamHI-HF and 10U XhoI enzymes. The rCutSmart buffer (NEB, Cat#B6004S) was used to buffer the reaction to ensure maximum enzyme activity and prevent star activity during extended incubation. Gel-isolated insert DNAs were also digested using BamHI-HF and XhoI restriction enzymes and rCutSmart buffer to create DNA overhangs for 1 h at 37ºC. Digested pCS2+ and pCDNA3.1+ were visualized by agarose gel electrophoresis using a 1.2% agarose gel prepared with ethidium bromide as single bands and were excised and extracted using the NucleoSpin PCR and Gel Clean Up Kit. The digested inserts were column-purified from excess enzymes and salts using the same kit.

Ligation reactions were performed using the Quick Ligation Kit (NEB, Cat#M2200S) by incubating for 15 min at room temperature (RT) or T4 DNA Ligase (NEB, Cat#M0202S) by overnight incubation at 16ºC.

2.2.4 Transformation and Plasmid Isolation

For normal cloning, chemically competent bacterial strain, DH5α, was transformed by heat-shock. 5 µl from ligation reactions were incubated with 50 µl of competent cells for 30 minutes on ice and subjected to heat-shock for 1 minute at 42°C by submersion in a warm water bath, then incubated for 2 minutes on ice. After transformation, the bacteria were incubated for 1 hour in fresh LB broth (Difco, Cat#244620) at 37 °C with shaking at 225 rpm to allow recovery and expression of ampicillin resistance proteins. Following this, the bacteria were pelleted by 2-minute centrifugation at 7,000 ×g and plated on fresh LB Agar Miller (Difco, Cat#244520) plates containing 100 µg/ml ampicillin (Goldbio Cat#A-301-5) using single-use sterile bacterial spreaders (ISOLAB Cat#082.03.001). The plates were incubated overnight at 37ºC and were removed from the incubator after 16 hours of incubation.

For SDM cloning, XL10 Gold ultracompetent cells were first incubated with 2 µl of β-mercaptoethanol mix provided in the kit for 10 minutes, while swirling the cells every 2 minutes. After incubation with β-mercaptoethanol, 4 µl of the DpnI-treated product was used to transform XL10 Gold competent cells and incubated on ice for 30 minutes, followed by 30 seconds of heat shock at 42°C and 2 minutes of incubation on ice. 1 ml of fresh LB Broth was added to the transformed bacteria and incubated at 37ºC and 225 rpm for 1 hour. After the incubation, cells were pelleted at 7,000 ×g and plated on LB agar with ampicillin (100 µg/ml). The plates were incubated overnight at 37ºC and were removed from the incubator after 16 hours of incubation.

Small batches (mini culture) of bacterial culture were prepared by picking single bacterial colonies from the LB agar plates. Bacteria were expanded in 5 ml LB Broth supplemented with 100 µg/ml ampicillin at 37ºC and 225 RPM. Plasmid isolation from mini-cultures was performed using the NucleoSpin Plasmid Mini Kit (Macherey-Nagel, Cat#740588.50). Isolated plasmids were sequenced using the Sanger sequencing method to confirm the inserts. Sanger sequencing of the plasmids was performed using the

BigDye v3.1 Terminator Cycle Sequencing Kit (Applied Biosystems, Cat#4337455) and sequencing primers SP6 for forward reads and T7 for reverse reads. Thermal cycling settings are described in the table below. Sequences were analyzed using a 3500xL Genetic Analyzer (Applied Biosystems, Cat#4440471). After confirming the integrity of the inserts, larger batches (midi-culture) of bacterial culture were prepared. Transformed bacteria were expanded in 100 ml LB broth supplemented with 100 µg/ml ampicillin and incubated overnight (14–16 h) at 37 °C with shaking at 225 rpm. Then, bacterial cultures were pelleted by centrifugation at x g for x mins at 4ºC and plasmid isolation from midi-cultures was performed using the NucleoBond Xtra Midi Kit (Macherey-Nagel, Cat#740410.50). The accuracy of each plasmid was confirmed by targeted Sanger sequencing.

2.3 Minigene Assay

2.3.1 Insert Amplification for Minigene Assay

To check the effect of the splicing variants, we performed minigene assay. We have three reported splicing variants for *DESI1* exon 4 (*v*5) and exon 5 (*v*1, *v*6). To clone into the pSPL3 backbone, fragments containing the desired exon and its surrounding intronic regions were amplified by PCR using Q5 High Fidelity DNA Polymerase. To capture any potential splice-regulatory elements, primers targeting -500 bps to +500 bps surrounding the intronic regions of exon 4 and exon 5 of *DESI1* were designed. Additionally, to serve as a technical replicate, primers targeting -200 bps to +200 bps surrounding the intronic regions of *DESI1* exon 5 were designed. The primers incorporated restriction enzyme recognition sites for cloning purposes, with an EcoRI site included in forward primers and BamHI sites added to the reverse primers. The sequences of all primers are listed in Table 2.13. For the WT constructs, gDNA from WT controls was used as a template, while for the construct containing the c.413+1G>A variant, gDNA from patient-derived fibroblasts (F1:II.2) was used. For the other two variants (c.289C>T and c.291-4A>G), patient samples were not available; therefore, the variants were introduced into WT constructs by site-directed mutagenesis (SDM). The detailed protocol is provided in Section 2.2.2.4, and the sequences of the SDM primers are listed in Table 2.10.

PCR clean-up of the reactions was performed using the NucleoSpin PCR and Gel Clean Up Kit according to the manufacturer's protocol. Purified DNA was eluted in a 30

µl volume. All amplified products were sequenced by Sanger sequencing to confirm the absence of additional mutations apart from the variant of interest.

Primer Name	Primer Sequence	Target
DESI1-Minigene-F1	ACGTACGTGAATTCGCTCTAAGTTGTTCTGATACAGATA	DESI1 Exon 5 and surrounding introns (500bp)
DESI1-Minigene-R1	ACGTACGTGGATCCTCGAGCACAATGGGAAGG	DESI1 Exon 5 and surrounding introns (500bp)
DESI1-Minigene-F2	ACGTACGTGAATTCTTGAGCAGATTTTCTCTGAAAGAGG	DESI1 Exon 5 and surrounding introns (200bp)
DESI1-Minigene-R2	ACGTACGTGGATCCTGGAGGTAATACAGGTGCGC	DESI1 Exon 5 and surrounding introns (200bp)
DESI1-Minigene-F3	ACGTACGTGAATTCATTCTTCATCTGCCCAGGGT	DESI1 Exon 4 and surrounding introns (500bp)
DESI1-Minigene-R3	ACGTACGTGGATCCCCCCGTCTCATACACCAGAA	DESI1 Exon 4 and surrounding introns (500bp)

Table 2.13: Cloning Primers for Minigene

Component	Volume
Q5 Reaction Buffer (5x)	5 µl
dNTP	0.5 µl
F primer	1.25 µl
R primer	1.25 µl
gDNA template	x µl (200 ng)
Q5 High Fidelity Polymerase	0.25 µl
ddH20	to 25 µl

Table 2.14: Q5 HF DNA Polymerase Reaction Mix for Minigene Inserts

Step	Temperature (°C)	Duration	Cycle
1	98	2 minutes	1
2	98	10 sec	35
3	63	30 sec	
4	72	30 sec	
5	72	2 minutes	1
6	4	Hold	1

Table 2.15: Q5 HF DNA Polymerase Thermal Cycling Conditions for Minigene Inserts

To create overhangs for cloning, restriction enzyme digestion was performed on 1000 ng of each amplified insert using 10U EcoRI (NEB, Cat#R0101S), 10U BamHI (NEB, Cat# R0136S) for 1 hour at 37°C. NEBuffer™ r2.1 Buffer (NEB, Cat#B6002S) was used for the reaction.

2.3.2 Cloning into pSPL3 Vector

The pSPL3 backbone is a specialized vector widely used for splicing analysis. The backbone contains two exons with intact splice acceptor and splice donor sites and a functional intron. A multiple cloning site (MCS) is present within the intron and allows for insertion of a target (Thompson & Young, 2017).

A total of 1000 ng of the empty pSPL3 backbone was digested by EcoRI and BamHI-HF to create overhangs compatible with the inserts. Due to incompatibility in digestion efficiency of enzymes in available buffers, sequential overnight digestions were performed. Firstly, the empty vector was digested with 10U EcoRI, using NEBuffer™ r2.1 Buffer for 16 hours at 37°C. The single-digested vector was purified using the NucleoSpin PCR and Gel Clean Up Kit according to the protocol. Purified DNA was eluted in a 30 µl volume and used for second overnight digestion with 10U BamHI-HF enzyme, using rCutSmart Buffer. Following this, the digested empty backbone was visualized by agarose gel electrophoresis using a 1.2% agarose gel prepared with ethidium bromide (EtBr) and 0.5% TBE Buffer. A 1 kb (NEB, Cat# N3232S) and a 100 bp DNA

ladder (Invitrogen, Cat#15628019) were used, and the corresponding band at approximately 6 kb was excised from the agarose gel using sterile scalpels. Gel excision of the digested plasmid was performed to prevent contamination with undigested or incompletely digested vectors.

Ligation reactions were performed using T4 DNA Ligase (NEB, Cat# M0202S) by overnight incubation at 16ºC. The backbone to insert ratio was 1:10 for the reaction. Reaction details are presented in Table 2.16.

Component	**Volume**
T4 DNA Ligase Buffer (10X)	2 µl
Vector DNA	x µl (50 ng)
Insert DNA	x µl (80 ng*) x µl (55 ng**)
Nuclease-free water	to 20 µl
T4 DNA Ligase	1 µl

Table 2.16: Ligation Reaction for Minigene Inserts

*Mass of DNA used for Exon 5 Set 1 **Mass of DNA used Exon 5 Set 2

2.3.3 Splicing Analysis-Minigene Assay

To determine the impact of intronic *DESI1* mutations on splicing, minigene assays were performed using the pSPL3-DESI1 Exon constructs created. HEK293T cells were transfected with 1 µg of wildtype and mutant minigene constructs, alongside empty pSPL3 vector as a control, using Lipofectamine 2000 (Invitrogen, Cat#11668-27) at a 1:3 DNA to reagent ratio. After 24 hours, cells were harvested for RNA extraction using the RNeasy Mini Kit (Qiagen, Cat#74104). cDNA was synthesized using the iScript Reverse Transcription Supermix (Bio-Rad, Cat#1708841). The resulting cDNA was used for RT-PCR using vector-specific primers (SD6-SA2), and splicing products were visualized with 1.2% agarose gels containing EtBr, at 120V for 30 minutes. Aberrant splicing was identified by comparing band sizes between wildtype and mutant RT-PCR bands.

2.4 Cell Culture, Transfection and Total Protein Isolation

Complete culture medium consisting of DMEM (4.5g/L) (Multicell, Cat#319-005 CL) supplemented with 10% fetal bovine serum (Biowest, Cat#S1620) and 1X penicillin-streptomycin antibiotics was used to culture patient primary fibroblasts and HEK293T cell lines. Cells were maintained in a humidified CO2 incubator at 37°C with 5% CO2. Primary patient fibroblasts were cultured in sterile T75 flasks (Sarstedt, Cat#83.3911), while HEK293T cells were cultured in sterile TC-100 dishes (Sarstedt, Cat#8339.02).

For transfection experiments, HEK293T cells were seeded in 6-well plates (Sarstedt, Cat#8339.20) and transfected upon reaching 80% confluency. Chemical transfection was performed using either Lipofectamine 2000 (Invitrogen, Cat# 11668-027) or FuGENE HD (Promega, Cat# E231) with DNA to reagent ratios ranging from 1:1 to 1:3 (µg: µl).

Cells were harvested 48 hours post-transfection by trypsinization using 0.05% Trypsin-EDTA (Multicell, Cat#325-542 EL) for 1 minute. Trypsin was neutralized with complete medium at a 1:2 ratio, and cells were collected in 15 ml centrifuge tubes (Sarstedt, Cat#62.554.502) and pelleted by centrifugation at 600×g for 5 minutes. Following supernatant removal, cell pellets were washed twice with cold PBS and centrifuged under the same conditions at 4°C.

Total protein isolation was performed using 1X RIPA lysis buffer (Ecotech, Cat#RIPA-100) supplemented with 1X protease inhibitor (PI) cocktail (Roche, Cat#11873580001) and 1 mM PMSF (Sigma-Aldrich, Cat#P7626-1G) to prevent protein degradation. Washed cell pellets were resuspended in RIPA lysis buffer, transferred to microcentrifuge tubes, and incubated on ice for 30 minutes. Following incubation, samples were centrifuged at 17,000×g for 30 minutes at 4°C. The resulting supernatant was transferred to low-protein binding microcentrifuge tubes (Sarstedt, Cat#72.706.600) and stored at -80°C until use.

2.5 Immunoblotting and Co-Immunoprecipitation

2.5.1 Immunoblotting

Protein samples were reduced and denatured using Laemmli buffer (Bio-Rad, Cat##1610747) with 50 mM DTT and boiled for 10 minutes at 95°C and then loaded into wells of precast 4-20% Tris-Glycine PAGE gels (Bio-Rad, Cat# 5671093) along with

protein ladder (Bio-Rad, Cat# 1610374) to check the corresponding size of the proteins. Electrophoresis was performed in the Tris-Glycine-SDS buffer at 120V for 90 mins. Proteins were transferred to PVDF membranes (Bio-Rad, Cat#1620175) using the semi-dry transfer method with the Trans-Blot Turbo Transfer System (Bio-Rad, Cat#1704150) and blocked using 5% non-fat milk powder in the TBST buffer for 1 hour at RT to prevent nonspecific binding. After blocking the membranes, incubation with primary antibodies at 4°C overnight was performed. All antibodies and their working dilutions are listed in Table 2.17.

Antibody	**Dilution**	**Host**	**Type**	**Catalog**
Anti-DESI1	1:500	Rabbit	Primary	Invitrogen Cat#PA5-62786
Anti-Ubiquitin	1:500	Mouse	Primary	Cell Signaling Technology Cat# 3936S
Anti-GAPDH	1:500	Mouse	Primary	Santa Cruz Biotechnology Cat# sc-47724
Anti-MYC	1:1000	Mouse	Primary	Cell Signaling Technology Cat# 2276S
Anti-FLAG	1:1000	Rabbit	Primary	Cell Signaling Technology Cat# 2368S
Anti-HA	1:1000	Rabbit	Primary	Sigma Cat#H6908-100UL
Anti-Mouse HRP	1:2000	Goat	Secondary	Abbkine Cat# A21010
Anti-Rabbit HRP	1:2000	Goat	Secondary	Abbkine Cat# A21020

Table 2.17: Immunoblotting Antibodies and Working Dilutions

2.5.2 Co-Immunoprecipitation

Co-immunoprecipitation experiments were performed using either anti-FLAG antibody-conjugated agarose beads (Sigma Aldrich, Cat#A2220-1ML) or anti-MYC antibody-conjugated magnetic beads (MedChemExpress, Cat# HY-K0206). Prior to use all beads were washed three times with RIPA buffer. Magnetic beads were collected using a magnetic rack, while agarose beads were pelleted by centrifugation 3,300 × g for 1 min at 4°C during sample preparation.

For *in vivo* interaction assays, HEK293T cells were co-transfected (described in Section 2.4) with plasmids encoding the ORF of target proteins Protein extraction from transfected cells was performed as described in Section 2.4. Transfection success and target protein expression levels were assessed by immunoblotting, and input amounts were adjusted to normalize protein concentration across samples. Normalized lysates were incubated with antibody-conjugated beads and rotated overnight (16 h) at 4°C.

For *in vitro* interaction assays, HEK293T cells were transfected with plasmids encoding the ORF of target proteins in separate wells. Transfection success and protein expression levels were assessed by immunoblotting, and input amounts were normalized prior to use. The bait protein, carrying the epitope tag recognized by the beads, was first incubated with antibody-conjugated beads for 6 h at 4°C on a rotating shaker. Beads were then washed three times with RIPA buffer supplemented with 1× PI cocktail and 1 mM PMSF to remove unbound proteins. Following this, lysates containing the prey protein were added, and incubation was continued overnight (16 h) at 4°C on rotating shaker to allow interaction of the proteins.

Following the overnight incubation in both methods, beads were washed three times with RIPA buffer supplemented with 1× PI cocktail and 1 mM PMSF prior to elution. Bound proteins were eluted by adding 50 µL of 2× Laemmli sample buffer supplemented with 60 mM DTT and heating at 95°C for 10 min. Eluate were subjected to immunoblotting as described in 2.5.1 to determine protein–protein interactions.

2.6 Immunofluorescence (IF) Staining and Confocal Imaging

For immunofluorescence analysis, patient-derived and WT primary fibroblasts of similar passage number were seeded at a density of 20,000 cells per well in 8-chamber immunofluorescence slides (Millipore, Cat#PEZGS0816) for 24 hours in humidified CO2 incubator at 37°C with 5% CO2. After incubation, the cells were washed twice with phosphate-buffered saline (PBS) (Biowest, Cat#L0615) and fixed with 4% paraformaldehyde (PFA) for 20 minutes at RT. Subsequently, the cells were blocked with 1% bovine serum albumin (BSA) in PBS for 1 hour at RT. Primary antibody incubation was performed overnight at 4°C, followed by three washes with 1% BSA in PBS. For double immunostaining, the cells were incubated with the second primary antibody for 2 hours at RT, followed by three additional washes with 1% BSA in PBS. Secondary antibody incubation was carried out for 1 hour at RT, followed by three washes with PBS. All antibodies and their working dilutions are listed in Table 2.18. Nuclear staining was performed using DAPI in (1:1000 dilution) PBS for 20 minutes, followed by three final PBS washes. Cells were mounted using ProLong Diamond Antifade Mounting Medium (Thermo Fisher Scientific, Cat#P36961).

Confocal imaging was performed using a Leica DMi8 inverted microscope equipped with SP8 confocal scanner. Imaging was performed at 40x magnification.

Antibody	**Dilution**	**Host**	**Type**	**Catalog**
Anti-Ub	1:500	Mouse	Primary	Cell Signaling Technology Cat# 3936S
Anti-Mouse Alexa Fluor 594	1:2000	Donkey	Secondary	Invitrogen Cat#A21203

Table 2.18: Immunofluorescence Antibodies and Their Working Dilutions

2.7 MG-132 treatment

MG-132 treatment for proteasomal inhibition was performed with 10 μM MG-132 (Sigma-Aldrich, Cat#474790) in culture medium for either 12 or 18 hours of incubation for transfected cells in 6-well plates. For immunofluorescence experiments, cells were incubated with 40 μM MG-132 for 4 hours in culture medium. All MG-132 treatments were performed with DMSO as vehicle control.

Chapter 3:
RESULTS

3.1 Clinical and Molecular Data

3.1.1 Clinical Presentation of Index Case

The index case was a male patient of Albanian origin who was initially examined in the Neurology Department at Koç University Hospital by Prof. Piraye Oflazer, presenting with progressive neuromuscular symptoms beginning at age 40. His initial manifestations included myotonia, exercise-induced fatigue, and lower back pain, which were mild at onset. The clinical course demonstrated a slow but progressive worsening, with symptom severity gradually increasing over the years. The patient developed additional features, including lower extremity pain and difficulty climbing stairs, while ambulation capacity was still maintained. He also reported tingling sensations in the legs along with persistent back and lower limb pain.

First electromyography (EMG) performed at age 41 revealed evidence of polyneuropathy and myotonic discharges. By age 43, clinical examination demonstrated musculoskeletal abnormalities, including increased lumbar lordosis, and gait evaluation revealed a pelvic tilt. Neurological assessment identified lower extremity weakness, inability to perform tiptoe walking, symmetrical atrophy of the gastrocnemius muscles which became asymmetrical over the following two years. Examination at 45 years revealed positive Babinski reflex indicating upper motor neuron involvement, and progressive lower extremity weakness evidenced by atrophy in distal and proximal leg muscles, mild strength loss, and a positive Gowers' sign.

A comprehensive genetic diagnostic evaluation was conducted in the Medical Genetics Department at Koç University Hospital by Prof. Hülya Kayserili and Dr. Şahin Avcı, systematically excluding alternative neuromuscular disorders, including Pompe disease, myofibrillar myopathy, and myotonic dystrophy type 1 (DM1). DMPK triplet repeat analysis showed normal results (5/14 repeats), definitively ruling out DM1. Whole exome sequencing (WES) was performed, yet no known pathogenic variants related to myopathy were identified. However, a homozygous splicing variant (*v1: DESI1*$^{c.413+1G>A}$) in the *DESI1* gene (*MIM614637*) was discovered. Segregation analysis demonstrated that

both unaffected parents and his brother were heterozygous carriers, consistent with an autosomal recessive inheritance. The pedigree of the index case is shown in Figure 3.1, and the detailed clinical symptoms are summarized in Table 3.1.

Disease Progression	Progressive	Axial and lower limb weakness
UMN Findings	Babinski Reflex	Positive
	Spasticity	Mild
	Hyperreflexia	DTR: +++/+++
LMN Findings	Muscular Weakness	Progressive, lower limbs
	Muscular Atrophy	Progressive
	Fasciculations	Absent
Bulbar Signs	Dysphagia	Absent
	Dysarthria	Absent
Sensory	Polyneuropathy	Present
	Neuropathic Pain	Present
Cognitive	Impairment	No
	Behavioral changes	No
Muscle pathology	Creatine Kinase	885 U/L (Elevated)
	Muscle Biopsy	Neurogenic and Nonspecific Myopathy

Table 3.1: Index Patient's Clinical Manifestations. UMN: Upper Motor Neuron, LMN: Lower Motor Neuron, DTR: Deep Tendon Reflex, Creatine Kinase upper limit is 200U/L for males

3.1.2 Expansion of the DESI1 patient cohort

Through international collaboration with Prof. Henry Houlden and Dr. Reza Maroofian at University College London, UK, and via the Centogene and GeneMatcher platforms, six additional patients from five unrelated families of diverse geographical backgrounds were identified and included in this study. All affected individuals presented with a progressive ALS-like phenotype. WES had been performed in each case to identify the causative variants; no variants were found in known disease-associated genes, whereas all individuals carried *DESI1* variants.

DESI1 variants identified in our cohort include three splice-site variants (*v*1*:* *DESI1*$^{c.413+1G>A}$, *v*5: *DESI1*$^{c.290+2T>A}$, *v*6: *DESI1*$^{c.291-4A>G}$), two frameshift variants (*v*2: *DESI1*$^{c.322dupT}$, *v*4: *DESI1*$^{c.417delC}$) and a single nonsense variant (*v*3: *DESI1*$^{c.289C>T}$). Remarkably, one patient presented as a compound heterozygote, carrying both a splice-site and a nonsense variant (F3II:1, *DESI1*$^{v1/v3}$). The pedigrees and geographical origins of affected individuals are illustrated in Figure 3.1.

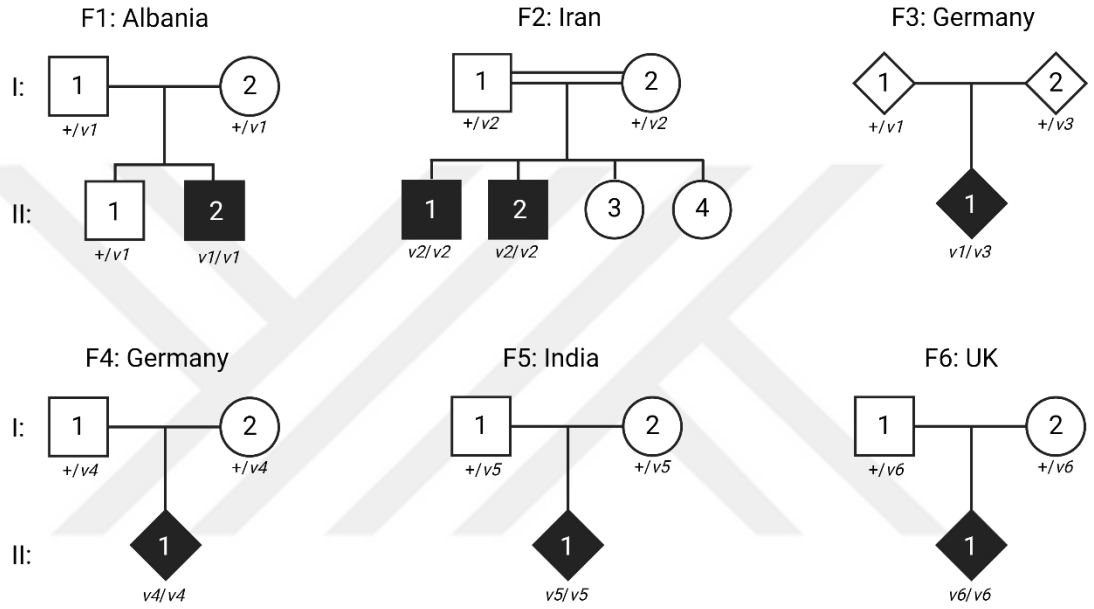

Figure 3.1: Pedigrees of Affected Individuals. Pedigrees from six unrelated families with affected individuals, consistent with autosomal recessive inheritance. Females are represented by circles, and males by squares. Diamond symbol represents an unspecified gender. Affected individuals are indicated by black-filled symbols. Families are labeled F1–F6, and generations are annotated using Roman numerals (I-II). Consanguineous marriages are depicted by double lines.

3.1.3 DESI1 Variants

In this study, we identified six *DESI1* variants located within exons 4-6 and their splice sites (Figure 3.2). Four of the six identified variants exhibit very low allele frequencies in the general population, while the remaining two are private variants, further supporting their potential pathogenicity. The variants are as follows:

- *v*1 (*DESI1*: c.413+1G>A) is located at the canonical splice donor site immediately downstream of exon 5.

- *v*2 (*DESI1*: c.322dupT; p. Cys108LeufsTer2) is a frameshift variant within the exon 5, introducing a premature stop codon.
- *v*3 (*DESI1*: c.289C>T; p. Arg97Ter) is a nonsense variant at the end of exon 4, resulting in the introduction of a premature stop codon.
- *v*4 (*DESI1*: c.417delC; p. Phe140LeufsTer57) is a single base deletion at the beginning of exon 6, resulting in frameshift that abolishes the canonical stop codon.
- *v*5 (*DESI1*: c.290+2T>A) affects the canonical splice donor site of exon 4, predicted to alter normal splicing patterns.
- *v*6 (*DESI1*: c.291-4A>G) resides within intron 4, adjacent to the splice acceptor site of exon 5, indicating a potential effect on normal splicing.

All the reported variants are expected to lead to severe alterations of the DESI1 protein, either through mis-splicing or by introducing truncation and stop loss, thereby highlighting *DESI1* as a strong causative candidate gene.

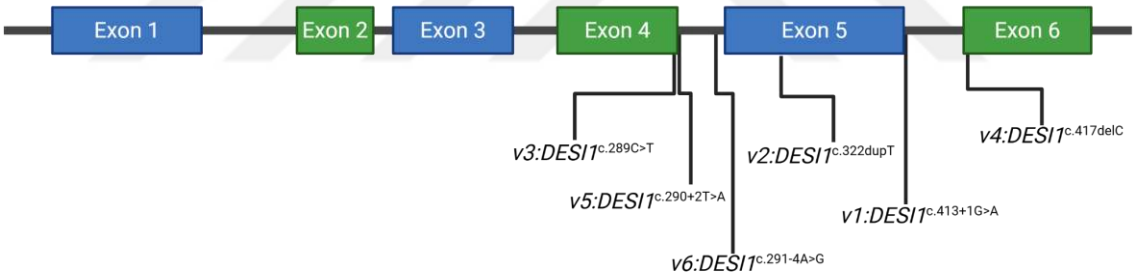

Figure 3.2: Schematic of DESI1 Gene structure and Locations of Identified Variants. DESI1 gene structure and variant positions. Exons 1-6 are shown as colored boxes connected by gray introns. Positions of reported variants are indicated by vertical black lines.

3.2 Pathogenicity Analysis of DESI1 Variants

3.2.1 In silico Pathogenicity Predictions for DESI1 Variants

In silico analysis of *DESI1* variants performed using MutationTaster (mutationtaster.org/), CADD (cadd.gs.washington.edu/), DANN (cbcl.ics.uci.edu/public_data/DANN/), phyloP (genome.ucsc.edu/cgi-

bin/hgTrackUi?db=hg38&g=cons100way) and SpliceAI (spliceailookup.broadinstitute.org/) where applicable. ExPASy Translate tool (web.expasy.org/translate/) was used to assess the resulting protein sequences from frameshift and nonsense variants and allele frequencies were derived from gnomAD (gnomad.broadinstitute.org/).

Variants that reside in the canonical splice donor sites, c.413+1G>A (*v*1) and c.290+2T>A (*v*5), were predicted to result in splice alterations, with splice-altering scores of 0.99 for both variants (>0.8 indicates high confidence for splice alteration), strongly suggesting disruption of normal splicing patterns. By contrast, the c.291-4A>G (*v*6) variant residing in the splice acceptor site, was predicted to be likely benign, with splice-altering score of 0.01 (<0.2 very unlikely to alter splicing). Both the frameshift c.322dupT (*v*2) and nonsense c.289C>T (*v*3) variants resulted in premature stop codons, leading to truncated proteins. *In silico* analysis further indicated deleterious effects for c.322dupT (*v*2) with a 1.0 score by MutationTaster (highest confidence in pathogenicity) as well as c.289C>T (*v*3) variant. These truncated proteins lack the C-terminal of the protein containing critical functional motifs as well as the catalytic cysteine residue. Conversely, the c.417delC (*v*4) frameshift variant results in a stop loss variant rather than a premature stop gain. This frameshift variant altered the amino acid sequence of the C-terminal entirely, extending the protein by an additional 27 amino acids and producing an aberrant C-terminal. *In silico* analysis also predicted this variant to be deleterious. Detailed results of *in silico* predictions are presented in Table 3.2.

Variant	**cDNA Coordinates**	**Variant Type**	**Prediction Tools**	**AF**	**Summary**
v1	c.413+1G>A	Splice donor	CADD: 34, SpliceAI: 0.99 DANN:1.0, MT:0.8	3.1×10^{-6}	Deleterious/ Splice Altering
v2	c.322dupT	Frameshift	MT: 1.0, ExPASy: Stop Gain	Private	Deleterious/ Truncating
v3	c.289C>T	Nonsense	CADD: 38, DANN:1.0 MT: 1.0 phyloP: 6.87, ExPASy: Stop Gain	1.9×10^{-5}	Deleterious/ Stop Gain

v4	c.417delC	Frameshift	DANN: 1.0, phyloP: 3.64, ExPASy: Stop Loss	6.2×10^{-7}	Deleterious/ Stop Loss
v5	c.290+2T>A	Splice donor	SpliceAI: 0.99, MT: 0.8, DANN:1.0	Private	Deleterious/ Splice Altering
v6	c.291-4A>G	Intronic	CADD: 4.8, SpliceAI: 0.01	1.2×10^{-6}	Likely Benign

Table 3.2: In silico Predictions of DESI1 Variants Pathogenicity AF: Allele frequency, CADD: Combined Annotation Dependent Depletion, >30 indicates deleterious; DANN: Deep Artificial Neural Network, >0.9 indicates deleterious; MT: MutationTaster >0.5 indicates disease causing; phyloP: >3.0 indicates conservation; ExPASy: ExPASy Translate Tool.

3.2.2 Analysis of Splice-Site Variants

3.2.2.1 *Validation with Minigene Assay*

Minigene assays are well-established methods frequently used to investigate splice site variants *in vitro*. The assay involves the cloning of the splice site variant with the affected exon and its surrounding introns inside an exon-trapping vector for its transient expression. If the cloned region contains a functional splice-site, it will be included between the vector's exons and will be detected by RT-PCR. Therefore, to functionally validate the impact of the three splice-site variants identified in our patient cohort (*v1*, *v5* and *v6*), we have generated pSPL3 exon-trapping WT and mutant constructs. The accuracy of the constructs is validated by targeted Sanger sequencing (Figure 3.3). All successfully generated minigene constructs are listed in Table 3.3.

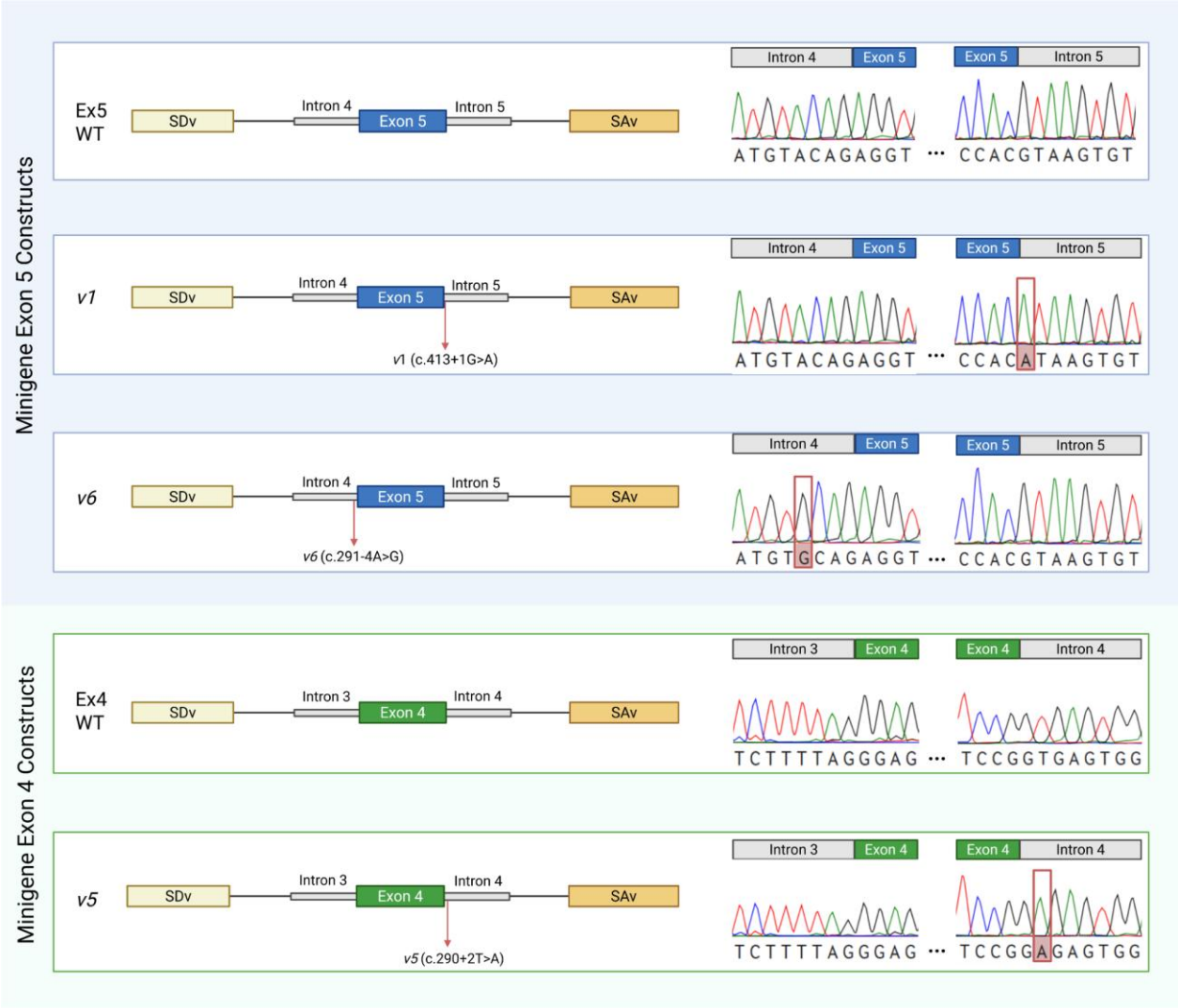

Figure 3.3: Validation of Minigene Constructs. The chromatogram sequencing confirmed the integrity of WT (Ex4 & Ex5) and mutant (v1, v6 and v5) minigene constructs. Red arrows indicate the position of the variant while red squares indicate the base change in the chromatogram. Ex: Exon

Construct name	Variant	Insert	Targeted Region	Vector	Template Source
Minigene Exon 5 WT Set1	WT	*DESI1* Exon 5	-500 to +500 bp surrounding intronic region	pSPL3	gDNA Amplification
Minigene Exon 5 WT Set2	WT	*DESI1* Exon 5	-200 to +200 bp surrounding intronic region	pSPL3	gDNA Amplification
Minigene Exon 5 c.413+1G>A Set1	V1	*DESI1* Exon 5	-500 to +500 bp surrounding intronic region	pSPL3	gDNA Amplification
Minigene Exon 5 c.413+1G>A Set2	V1	*DESI1* Exon 5	-200 to +200 bp surrounding intronic region	pSPL3	gDNA Amplification
Minigene Exon 4 WT	WT	*DESI1* Exon 4	-500 to +500 bp surrounding intronic region	pSPL3	gDNA Amplification
Minigene Exon 4 c.290+2T>A	V2	*DESI1* Exon 4	-500 to +500 bp surrounding intronic region	pSPL3	SDM of Minigene Exon 4 WT

Table 3.3: List of Minigene Constructs

Following the successful generation of the pSPL3 WT and mutant DESI1 minigene constructs, HEK293T cells were transfected with the constructs, including empty pSPL3 as a negative control. 24 hours post-transfection, RT-PCR analysis revealed distinct splicing patterns between the WT-Ex5 and *v1* constructs, as well as between the WT-Ex4 and *v5* constructs (Figure 3.4). Transfection with the WT-Ex5 construct generated a 386 bp product, consistent with exon 5 inclusion in the mature transcript. In contrast, the *v1* variant produced a 263 bp product, identical to the empty pSPL3 control, indicating complete exon 5 skipping. This aberrant splicing pattern was consistently observed in both *v1* minigene sets, containing 200 bp and 500 bp of intronic sequences, respectively (Figure 3.4), confirming that the splicing defect originates from the disrupted splice donor site rather than distal regulatory elements.

Transfection with the WT-Ex4 construct yielded a 373 bp product, consistent with exon 4 inclusion, while the *v5* variant resulted in a 263 bp product identical to the empty control, indicating exon 4 skipping. A schematic representation of the splicing events is provided in Figure 3.4.

To validate these findings, RT-PCR products were excised from the gel and subjected to Sanger sequencing. Sequencing of the 386 bp WT-Ex5 product confirmed the inclusion of DESI1 exon 5 between the vector exons (SDv and SAv), whereas sequencing of the 263 bp *v1* product revealed complete exon 5 skipping with direct SDv-SAv fusion. Similarly, sequencing of the 373 bp WT-Ex4 product confirmed exon 4 inclusion, while the *v5* variant showed a truncated 263 bp band consistent with exon 4 skipping. Representative sequencing chromatograms displaying exon–exon junctions are shown in Figure 3.4.

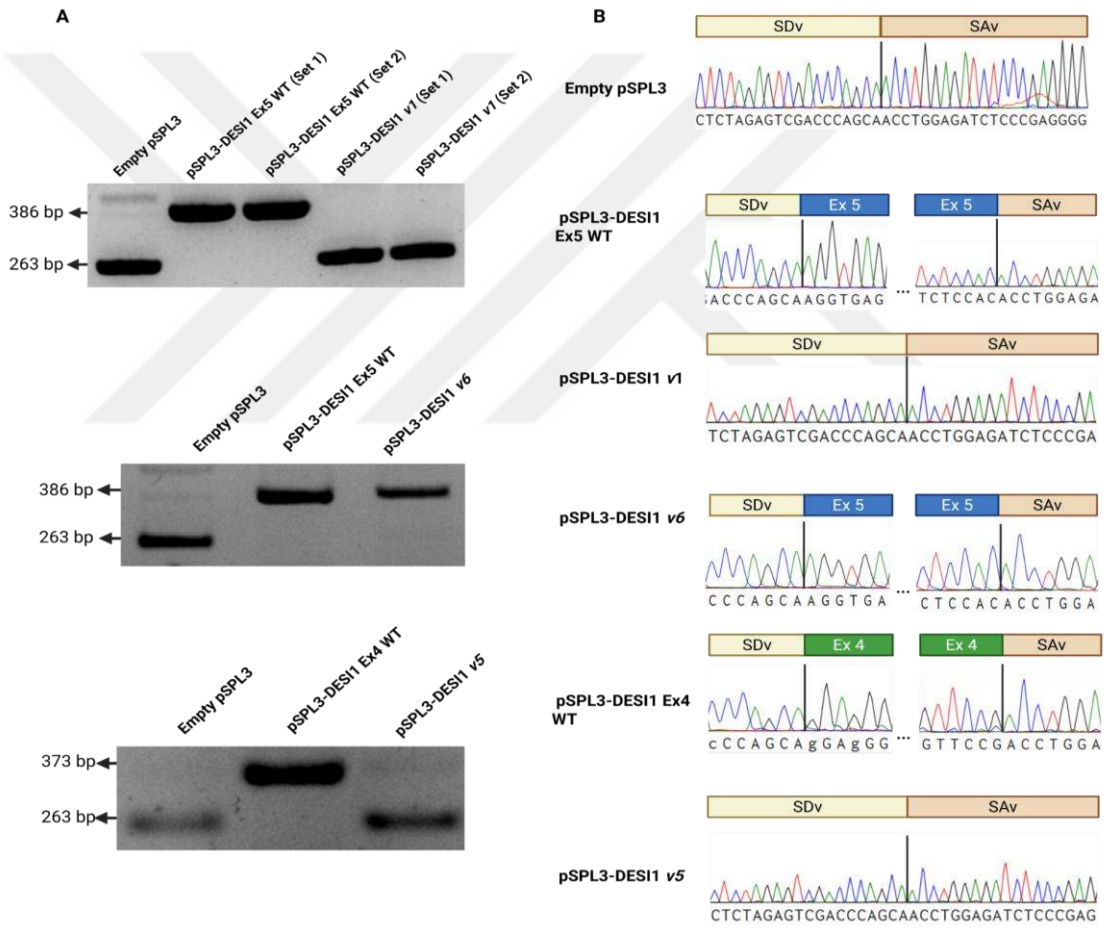

Figure 3.4: RT-PCR Minigene Assay for Splicing Validation and Sanger Sequencing of Excised Bands. A) HEK293T cells were transfected with pSPL3 constructs containing either wild-type (WT) Exon 5 or Exon 4, or patient-specific variant constructs (v1 and v6 affecting Exon 5; v5 affecting Exon 4). RT-PCR products were separated by agarose gel electrophoresis to assess splicing patterns. B) Sanger sequencing chromatograms of excised bands, shown from top to bottom, confirm the splicing outcomes: empty pSPL3 vector (no exon insertion), WT Exon 5 construct (correct exon 5 inclusion), DESI1-v1 (exon 5 skipping and junction of vector exons) and v6 constructs (correct exon 5

inclusion), WT Exon 4 construct (correct exon 4 inclusion), and DESI1-v5 construct (exon 4 skipping and junction of vector exons). Black lines indicate exon–exon junctions.

3.2.2.2 *v1* Splice-Site Variant validation with RT-PCR

To validate whether the splicing defect observed in the minigene assay is also present in the patient primary cells, we performed RT-PCR analysis using available patient (F1:II.2) primary fibroblasts, harboring *v1* splice-site variant. For RT-PCR amplification, we used primers targeting exon 4 and exon 6 (Figure 3.5). RT-PCR products from WT cells showed approximately 247 bp band on agarose gel electrophoresis, consistent with normal splicing (exon 5 inclusion). In contrast, RT-PCR from F1:II.2 patient cells yielded a smaller product, approximately 124 bp, consistent with complete exon 5 skipping from the mature *DESI1* transcript (Figure 3.5). Complete exon 5 skipping was further confirmed by Sanger sequencing of the gel-excised RT-PCR products. The WT products included exon 5 and showed expected exon junctions in the mature transcript, while RT-PCR products from patient F1:II.2 showed a direct junction of exons 4 and 6, confirming exon 5 skipping in the patient (Figure 3.5).

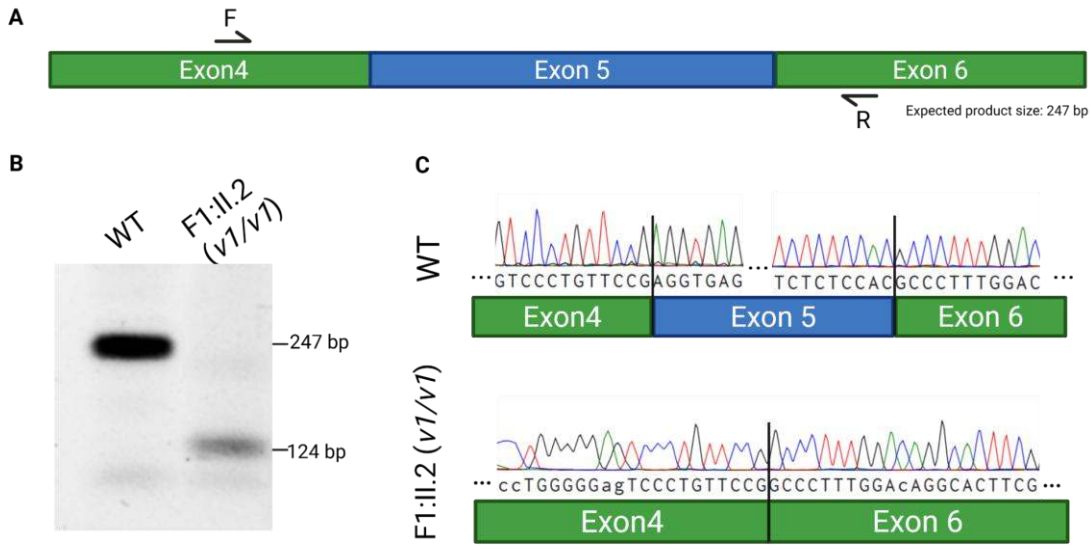

Figure 3.5: The v1 variant causes exon 5 skipping in patient-derived fibroblasts. A) Schematic representation of DESI1 exons 4-6 showing primer locations used for RT-PCR (F: forward primer; R: reverse primer). B) RT-PCR analysis of DESI1 transcripts from patient F1:II.2 (v1) and WT primary fibroblasts. C) Sanger sequencing of excised DNA bands from RT-PCR analysis.

3.2.3 Functional Validation of DESI1 Loss-of-Function Variants

3.2.3.1 *Generation of Expression Constructs*

To investigate the functional consequences of *DESI1* variants, we generated an extensive set of expression constructs for both transient and stable overexpression studies. Full-length WT and mutant *DESI1* ORF sequences containing N-terminal epitope tags were successfully cloned into mammalian expression vectors pCS2+ and pcDNA3.1+.

Multiple epitope tags (MYC, FLAG, HA) were used to facilitate co-immunoprecipitation experiments. The pCS2+ backbone was utilized for transient transfection studies due to its established use in our laboratory. For generating stable DESI1-overexpressing cell lines, we used pcDNA3.1+, which contains the neomycin resistance gene (NeoR/KanR) necessary for antibiotic selection in mammalian cells. These constructs will be further used in subsequent experiments.

Template sources for each variant were determined by availability of patient's samples. For variant *v1*, from which we had available patient samples (F1:II.2), we directly amplified *DESI1* from patient cDNA to capture complete exon 5 skipped transcript. For variants from patients whose samples were unavailable, we used site-directed mutagenesis to introduce the mutations to the WT *DESI1*, where applicable.

Additionally, to investigate the effects of the variants on DESI1's protein interactions, we generated constructs for DESI1's known substrates and interaction partners. UBQLN1, BZEL, SUMO1, SUMO2 and SUMO3 were successfully cloned into pCS2+ vector, while the UBQLN2 and UBQLN4 plasmids used for the experiments were kindly gifted from Dr. Magdalena (University of Michigan, USA) and Dr. Hirayama (University of Tokyo, Japan), respectively.

All constructs were verified by targeted Sanger sequencing. The chromatogram sequencing results for *DESI1* mutant constructs (*v1, v2*, *v3* and *v4*) are shown in Figure 3.6 confirming the presence of epitope tags, exon 5 skipping (*v1*) and patient variants (*v2*, *v3* and *v4*). The complete list of expression constructs generated in this study is presented in Table 3.4.

Type of construct	Construct name	Variant	Tag	Insert	Vector	Template Source
WT DESI1 Constructs (Transient overexpression)	N-MYC-DESI1 WT	WT	MYC	*DESI1*	pCS2+	pCAG N-HA DESI1 (Gift from Dr. Hirayama)
	N-FLAG-DESI1 WT	WT	FLAG	*DESI1*	pCS2+	pCAG N-HA DESI1 (Gift from Dr. Hirayama)
	N-HA-DESI1 WT	WT	HA	*DESI1*	pCS2+	pCAG N-HA DESI1 (Gift from Dr. Hirayama)
DESI1 Variant Constructs (Transient overexpression)	N-MYC-DESI1 c.413+1G>A	*v*1	MYC	*DESI1*	pCS2+	cDNA of Patient F1:II.2
	N-FLAG-DESI1 c.413+1G>A	*v*1	FLAG	*DESI1*	pCS2+	cDNA of Patient F1:II.2
	N-HA-DESI1 c.413+1G>A	*v*1	HA	*DESI1*	pCS2+	cDNA of Patient F1:II.2
	N-MYC-DESI1 c.322dupT	*v*2	MYC	*DESI1*	pCS2+	SDM of pCS2+ N-MYC-DESI1-WT Construct
	N-FLAG-DESI1 c.322dupT	*v*2	FLAG	*DESI1*	pCS2+	SDM of pCS2+ N-FLAG-DESI1-WT Construct
	N-MYC-DESI1 c.289C>T	*v*3	MYC	*DESI1*	pCS2+	SDM of pCS2+ N-MYC-DESI1-WT Construct
	N-MYC-DESI1 c.417delC	*v*4	MYC	*DESI1*	pCS2+	SDM of pCS2+ N-MYC-DESI1-WT Construct
WT and Variant DESI1 Constructs (Stable/Transient overexpression)	N-MYC-DESI1 WT	WT	MYC	*DESI1*	pcDNA 3.1+	pCS2+ N-MYC- DESI1-WT Construct
	N-MYC-DESI1 c.413+1G>A	*v*1	MYC	*DESI1*	pcDNA 3.1+	pCS2+ N-MYC- DESI1-c.413+1G>A Construct
	N-MYC-DESI1 c.322dupT	*v*2	MYC	*DESI1*	pcDNA 3.1+	pCS2+ N-MYC- DESI1-c.322dupT Construct
DESI1 Interaction partners Constructs (Transient overexpression)	MYC-BZEL	WT	MYC	*BZEL*	pCS2+	cDNA of SH-SY5Y
	HA-SUMO1	WT	HA	*SUMO1*	pCS2+	cDNA of HEK293T
	HA-SUMO2	WT	HA	*SUMO2*	pCS2+	cDNA of HEK293T
	HA-SUMO3	WT	HA	*SUMO3*	pCS2+	cDNA of HEK293T
	FLAG-UBQLN1	WT	FLAG	*UBQLN1*	pCS2+	pCMV4+ N-FLAG UBQLN1 (Gift from Dr. Ivanova)

Table 3.4: List of Expression Constructs Generated for Functional Studies. SDM: Site-directed mutagenesis, "N-" indicates the tag is positioned at the N-terminal of the protein, MYC-tag: EQKLISEEDL, FLAG-tag: DYKDDDDK, HA-tag: YPYDVPDYA.

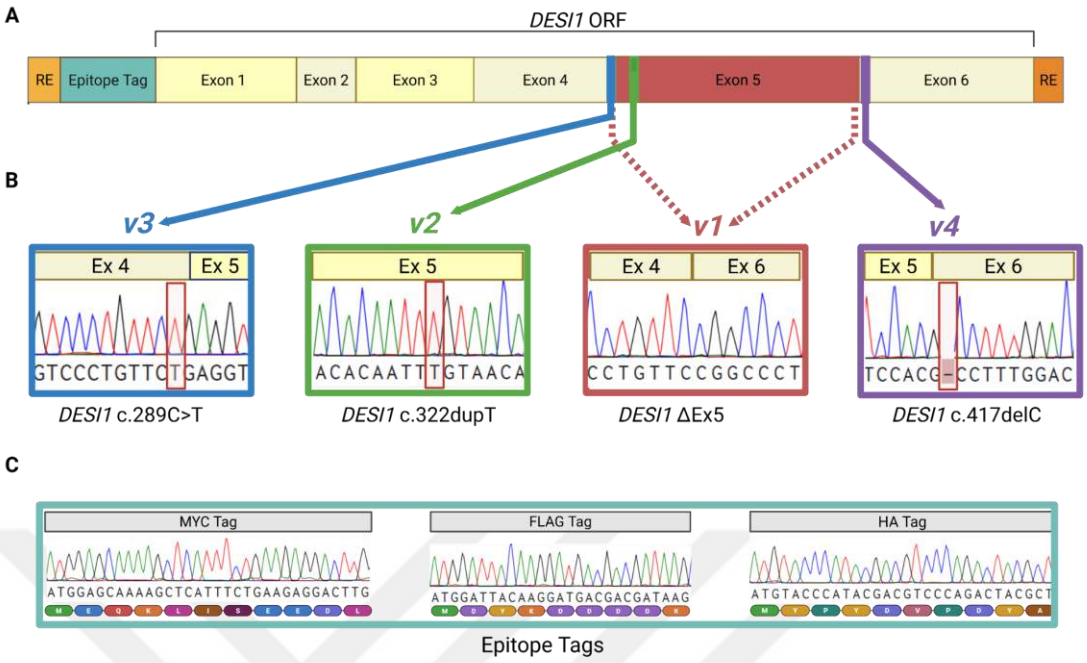

Figure 3.6: Validation of DESI1 (v1–v4) Constructs and Their Epitope Tags. A) Schematic representation of the affected exon 5 in the v1 construct as well as the locations of v2**,** v3, and v4 within the DESI1 ORF. B) Sequencing chromatograms confirming the accuracy of DESI1 mutant constructs. Red indicates the skipped exon 5 resulting from v1 (c.413+1 G>A); green indicates v2 (c.322dupT), successful insertion of a T nucleotide by SDM; blue indicates v3 (c.289C>T), successful C-to-T conversion by SDM; and purple indicates v4 (c.417delC), successful deletion of a C nucleotide by SDM. C) Chromatograms showing the validity of incorporated tags.

3.2.3.2 *DESI1 variants produce defective proteins missing key functional elements*

To understand the consequences of *DESI1* variants at the protein level, we analyzed their predicted translated protein using ExPASy and illustrated their structural alterations in Figure 3.7. WT DESI1 protein consists of one PPPDE domain and two nuclear export signal (NES) domains (NES1 and NES2). The PPPDE domain mediates the DeSUMOylase activity through Cys108-His38 catalytic dyad (Suh *et al*., 2012; Shin *et al*., 2012). The NES domains facilitate the nuclear export of polyubiquitinated proteins, with NES2 demonstrated to be functionally active (Hirayama *et al*., 2018).

Variant *v1*, which causes complete skipping of exon 5, produces an in-frame deletion that generates a truncated protein of 127 amino acids (p.Gly98_Thr138del). This truncation removes the catalytic cysteine at position 108, necessary for deSUMOylase

function, while retaining the NES2 sequence required for CRM1 recognition and nuclear export.

Variant *v2*, which causes a frameshift leading to premature stop codon (p.Cys108LeufsTer2), and variant *v3*, which introduces a nonsense mutation (p.Arg97Ter), produce truncated proteins of 108 and 96 amino acids, respectively. Both variants lack the catalytic cysteine residue as well as the NES2 sequence required for CRM1 recognition, and result in a complete loss of the C-terminus.

Variant *v4*, another frameshift variant, leads to a completely aberrant C-terminal sequence and extension of the protein by 27 amino acids due to the loss of the stop codon (p.Phe140LeufsTer57).

Variant *v5*, causes the skipping of exon 4, also introduces a premature stop codon (p.Gly61ArgfsTer2), resulting in severe truncation of the protein. The truncated protein is only 61 amino acids long, lacking all functional motifs.

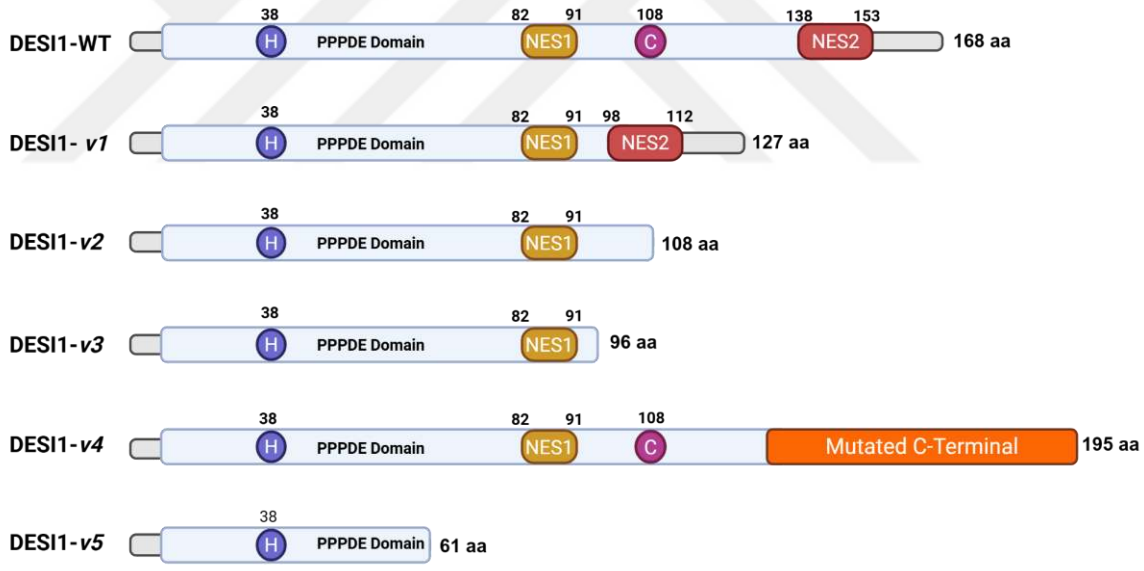

Figure 3.7:Protein Domain Architecture Schematic of DESI1 WT and Variants. The WT DESI1 protein contains a single PPPDE domain and two nuclear export signal (NES) domains (NES1 and NES2). Variants *v1, v2, v3*, and v5 result in truncated proteins, whereas variant *v4* leads to a protein extension, with all variants affecting the protein's functional domains.

To experimentally investigate the consequence of the variants with available overexpression constructs (*v1*-*v4*), we transfected the HEK293T cells with WT or mutant constructs. Following protein extraction, DESI1 protein levels were assessed using

western blotting. The results revealed truncated and highly degraded DESI1 proteins for the *v1*, *v2*, and *v3* variants. Consistent with our predictions, the *v4* variant produced an extended protein of higher molecular weight in lower amounts (Figure 3.8).

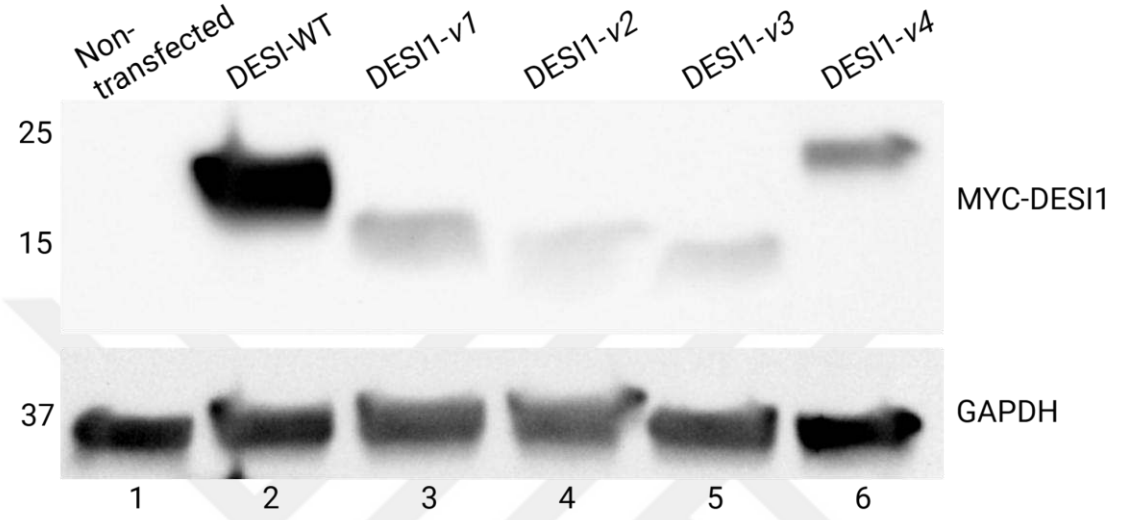

Figure 3.8: Western Blot Analysis of WT and Mutant DESI1 Overexpressed in HEK293T cells. The results showed truncated, highly degraded DESI1 proteins for v1, v2, and v3 compared to wildtype, while v4 produced a higher–molecular-weight protein with reduced abundance. GAPDH was used as a loading control.

To determine whether the degradation of *v1*, *v2*, and *v3* occurs via the proteasomal pathway, we treated transfected HEK293T cells with MG-132, a proteasomal inhibitor. Notably, DESI1 protein levels increased for *v1*, *v2*, and *v3* upon MG-132 treatment, confirming proteasome-mediated degradation. For *v4*, protein levels showed a slight increase after treatment, indicating that this variant is less prone to proteasomal degradation (Figure 3.9)**.**

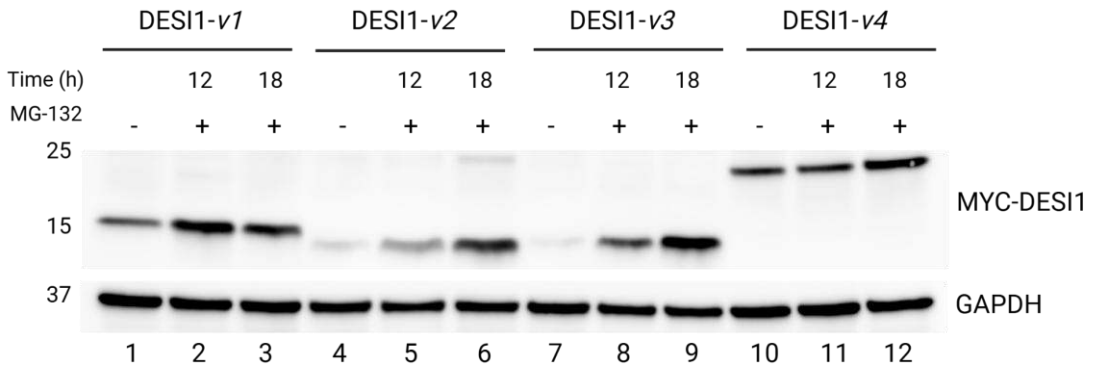

Figure 3.9: Western Blot Analysis of Mutant DESI1 Overexpression Samples Treated with MG-132 at Different Time Points. The results demonstrated a time-dependent accumulation of mutant DESI1 proteins (*v1, v2, v3*, and *v4* variants) under MG-132 treatment, indicating that these proteins undergo degradation via the proteasomal pathway.

3.2.3.3 *Loss-of-function validation of DESI1 variants in patient-derived primary fibroblasts*

In collaboration with our clinical partners, we obtained fibroblasts from two patients. The sample from Patient F1:II.2, carrying the *v1* pathogenic variant, was provided by Dr. Şahin Avcı at Koç University Hospital (Turkey). Fibroblasts from Patient F2:II.1, carrying the *v2* variant, were kindly provided by Dr. Reza Maroofian at UCL (UK). To assess *DESI1* expression in patient fibroblasts, we performed qPCR analysis using primers targeting the N-terminal region of the *DESI1* gene and Western blot analysis for endogenous DESI1 protein.

The preliminary qPCR results did not show a consistent pattern in *DESI1* mRNA levels between patients and WT control fibroblasts. In patient F1:II.2 carrying the *v1* variant, we observed similar *DESI1* transcript levels, while patient F2:II.1 carrying *v2* variant showed a significant increase compared to wild-type controls (Fig 3.10. A). However, Western blot analysis demonstrated a complete loss of DESI1 protein in both patient fibroblasts, consistent with the findings from the *v1*- and *v2*- overexpressed samples. Unlike overexpressed constructs, we could not detect truncated DESI1 protein (Figure 3.10 B, lanes 3 and 4), suggesting the degradation of the mutant proteins.

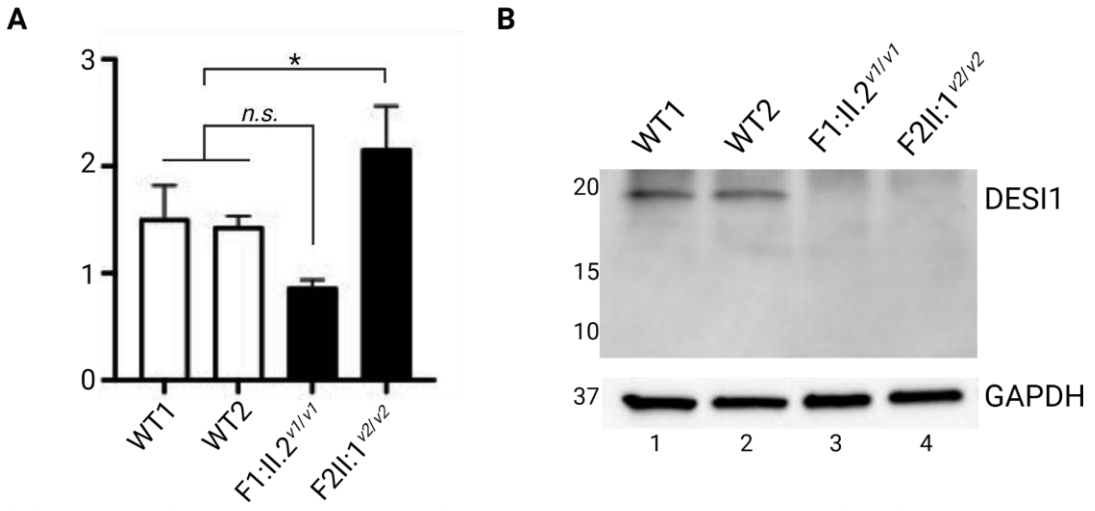

Figure 3.10: qPCR and Western Blot showing DESI1 expression in RNA and Protein Level. A) qPCR analysis of DESI1 showed a mild, non-significant decrease in patient F1:II.2 and a significant increase in patient F2:II.1 primary fibroblasts compared to the two wild-type controls. Statistical significance was assessed by Student's t-test (*p<0.05). n.s. = not significant, n=3. B) Western blot analysis of endogenous DESI1 protein (~20 kDa) using whole protein extracts from primary dermal fibroblasts from WT (WT1 and WT2) and patient F1:II.2 and F2:II.1 individuals. The results showed a complete absence of DESI1 protein in patient fibroblasts (Lanes 3 and 4). GAPDH served as a loading control.

3.3 Defective deSUMOylase Function of Mutant DESI1

To investigate whether *DESI1* variants affect it's deSUMOylase activity, we checked the enzymatic activity of the least truncated protein produced by the *v1* variant. This variant results in an 11–amino acid truncation of the PPPDE domain, which mediates substrate deSUMOylation. For this purpose, we performed an in vitro co-immunoprecipitation (co-IP) experiment using FLAG-DESI1-WT, FLAG-DESI1-*v1* (ΔEx5), MYC-BZEL and HA-SUMO1 constructs. BZEL, a transcription factor, is a known substrate of DESI1's deSUMOylase activity, and its deSUMOylation is essential for regulating its suppressor activity. To assess the molecular interaction between DESI1 and its substrate for deSUMOylation, HEK293T cells were co-transfected with MYC-BZEL and HA-SUMO1 to allow SUMOylation of BZEL, followed by *in vitro* co-IP with either FLAG-DESI1-WT or FLAG-DESI1-*v1* individually.

Co-IP using anti-MYC beads revealed a significant difference in the pulldown. DESI1-WT, co-immunoprecipitated with BZEL, indicating presence of enzyme-substrate interaction. However, DESI1-*v1* (ΔEx5) did not co-immunoprecipitate with BZEL.

Additionally, immunoblotting with anti-HA detected a higher molecular weight SUMO-BZEL conjugate that was much stronger in the immunoprecipitation with the DESI1-*v1* compared to DESI1-WT, providing strong evidence for the loss of deSUMOylase function in the mutant protein (Figure 3.11). Considering that the *v1* variant, which causes the least truncation of the PPPDE domain compared to *v2*, *v3*, and *v5*, exhibits defective deSUMOylase activity, we strongly infer that the other variants also lead to enzymatic dysfunction. Notably, for *v5*, the PPPDE domain remains intact; however, the presence of an aberrant C-terminal region may induce conformational changes that impair its deSUMOylase function. Additional co-IP experiments on the remaining mutant proteins are currently in progress.

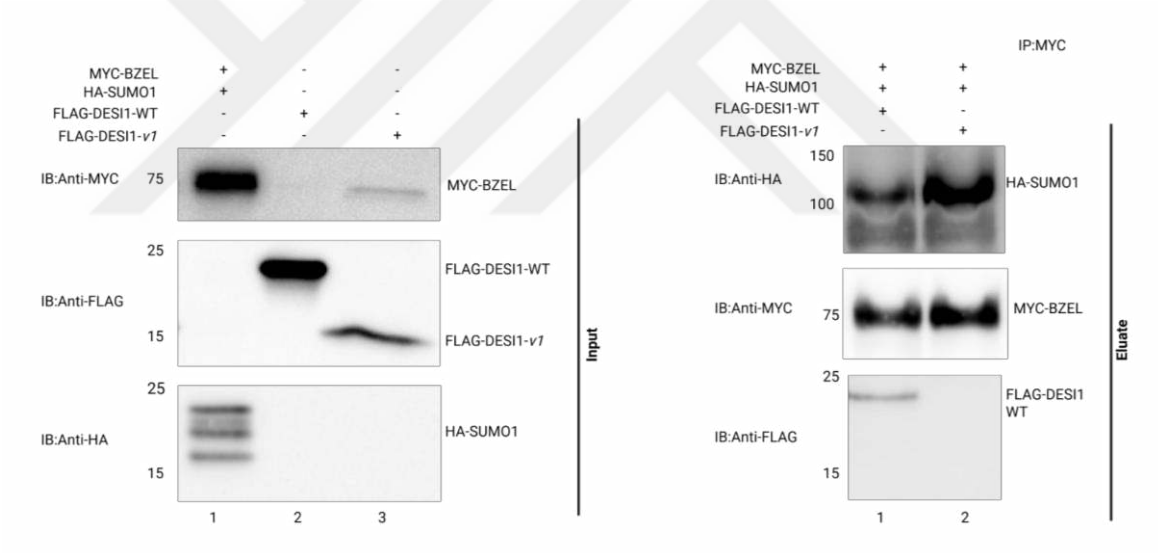

Figure 3.11: In vitro Co-IP assay to evaluate deSUMOylase function of DESI1. HEK293T cells were transfected with MYC-BZEL and HA-SUMO1, followed by in vitro co-IP using MYC beads with either FLAG-DESI1-WT or FLAG-DESI1-v1 individually. Input samples blotted with anti-MYC, anti-FLAG and anti-HA antibodies are shown on the left side. The IP results shown on the right side revealed a clear interaction between FLAG-DESI1-WT and MYC-BZEL (eluate, Lane 1) but not between FLAG-DESI1-v1 and MYC-BZEL (eluate, Lane 2). Notably, a stronger high–molecular weight SUMOylated BZEL band using anti-HA antibody was observed in the FLAG-DESI1-v1 (eluate, Lane 2) compared to FLAG-DESI1-WT (eluate, Lane 1), indicating defective deSUMOylase activity in the mutant protein.

3.4 Augmented interaction between mutant DESI1 and UBQLN4

DESI1 functions as a nuclear export adaptor for UBQLN proteins; however, the specific region mediating this interaction remains unknown. To assess how *DESI1* variants affect this interaction, we examined the least truncated protein produced by the *v1* variant. To evaluate how DESI1 variants affect this interaction, we examined the least truncated protein produced by the *v1* variant. HEK293T cells were co-transfected with MYC-tagged DESI1-WT or DESI1-*v1* (ΔEx5) constructs along with FLAG-UBQLN4, followed by *in vivo* co-IP using FLAG-beads. Surprisingly, the co-IP assays revealed a markedly stronger interaction between DESI1-*v1* and UBQLN4 compared to DESI1-WT.

To determine whether this augmented interaction was due to compensatory pathways in HEK293T cells or it is related to DESI1-*v1* protein structural changes, we next performed *in vitro* co-IP assays using individually transfected DESI1-WT, DESI1-*v1*, and UBQLN4 constructs. Consistently, DESI1-*v1* demonstrated a higher binding affinity for UBQLN4 compared to the DESI1-WT protein. These findings suggest that the truncated protein generated by the *v1* variant is structurally more prone to interact with UBQLN4. The results were reproducible across four *in vivo* and two *in vitro* co-IP experiments. Additional co-IP analyses of the remaining mutant proteins are currently ongoing.

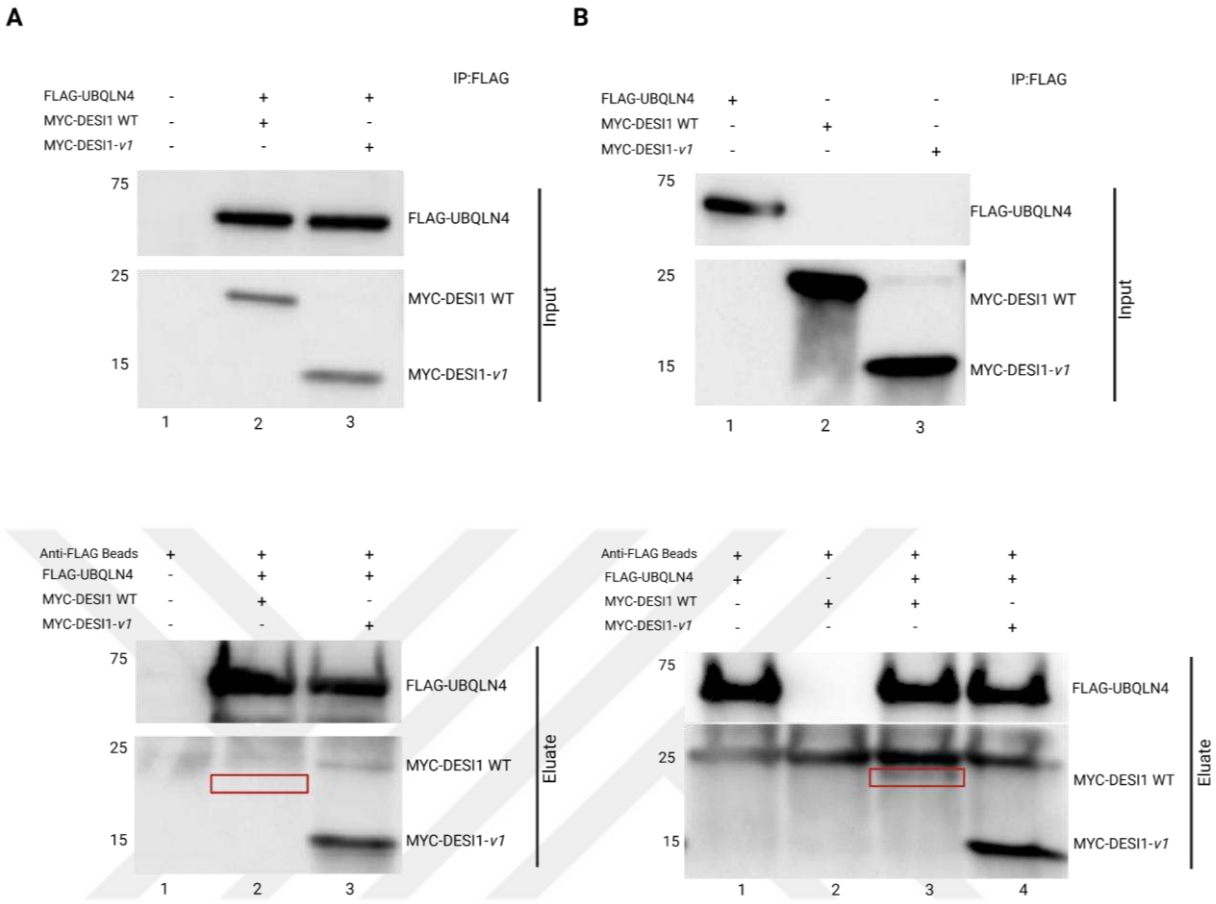

Figure 3.12: In vivo and in vitro Co-IP assays evaluating the interaction of DESI1 with UBQLN4. A) In vivo co-IP using FLAG beads revealed an increased interaction between DESI1-v1 and UBQLN4 (eluate, Lane 3) compared to DESI1-WT (eluate, Lane 2, expected position indicated by red box). Non-transfected sample served as negative control. B) In vitro co-IP using FLAG beads confirmed the stronger affinity of DESI1-v1 for UBQLN4 (eluate, Lane 3) compared to DESI1-WT (eluate, Lane 2, expected position indicated by red box). A single pull-down with either FLAG-UBQLN4 or MYC-DESI1-WT served as negative controls.

3.5 Defective Nuclear Export of Polyubiquitinated Proteins and Impaired Ubiquitin Recycling in DESI1 Patient Fibroblasts

To investigate the cellular consequences of DESI1 loss-of-function and the augmented interaction between DESI1-v1 and UBQLN4 on the nuclear export of polyubiquitinated proteins, we performed preliminary Immunofluorescence (IF) analysis using patient (F1:II.2) primary fibroblasts. To exacerbate proteostatic stress and reveal defects in protein clearance pathways, cells were treated with the proteasome inhibitor

MG-132 prior to staining. The analysis revealed an increased nuclear ubiquitin signal, indicating defective nuclear export and subsequent accumulation of polyubiquitinated proteins within the nucleus (Figure 3.13A). Quantification of the mean fluorescent intensity of nuclear ubiquitin signal revealed a significant increase in nuclear polyubiquitin in patient (F1:II.2) primary fibroblasts compared to wild-type controls (Figure 3.13B). To further assess whether impaired nuclear export disrupts ubiquitin recycling and reduces the pool of free ubiquitin, we examined free ubiquitin levels in available patient-derived primary fibroblasts (F1:II.2 and F2:II.1) using immunoblotting. Notably, a marked reduction in free ubiquitin levels was observed in both patient fibroblasts compared to two wild-type controls (Figure 3.13C).

Together, these findings establish that *DESI1* variants identified in our cohort cause loss of protein stability, abolish deSUMOylase activity, and perturb interactions with UBQLN4, thereby impairing the nuclear export of polyubiquitinated proteins and disrupting DESI1-mediated deSUMOylation.

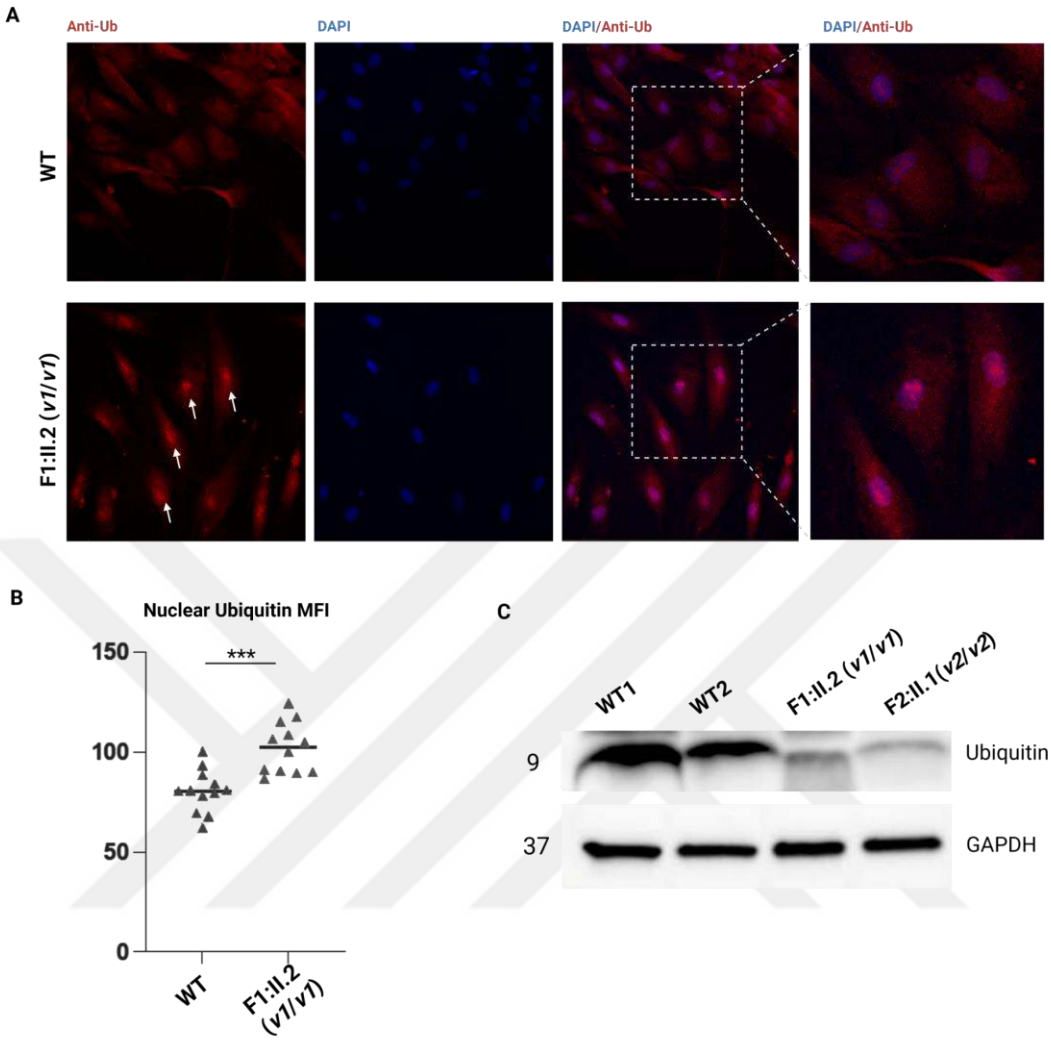

Figure 3.13: Immunofluorescence and Western blot analysis of ubiquitin turnover in WT and mutant primary fibroblast. A) Confocal microscopy images of primary fibroblast cells stained with DAPI (blue, nuclei) and anti-ubiquitin (anti-Ub, red). Arrows indicate nuclear ubiquitin aggregates in F1:II.2 cells. B) Quantification of nuclear ubiquitin mean fluorescence intensity (MFI) showed significantly elevated ubiquitin levels in F1:II.2 cells compared to WT. Statistical significance was assessed by Student's t-test (***$p<0.001$). C) Western blot results revealed a significant reduction in free ubiquitin levels in patients' primary fibroblasts (F1:II.2 and F2:II.2) compared to WT controls.

Chapter 4:
DISCUSSION & CONCLUSION

4.1 ALS relevance and clinical overlap

The patients described in this study presented with a combination of clinical features that strongly overlap with classical ALS. The progressive weakness and combined involvement of upper and lower motor neurons place this condition within the ALS disease spectrum. Importantly, upper motor neuron lesions, hallmarks of ALS were consistently observed across affected individuals. Although sensory involvement and the absence of fasciculations are atypical for ALS, the presence of positive Babinski reflex and hyperreflexia provide clear evidence for upper motor neuron (UMN) involvement. The adult-onset presentation also suggests an underlying process linked to age-related decline in proteostasis and neuronal homeostasis, converging on mechanisms relevant to ALS pathogenesis (Hipp *et al*., 2019).

Beyond the clinical resemblance, functional analyses highlight a mechanistic link between *DESI1* and ALS biology. DESI1 functions as a CRM1-dependent adaptor for the nuclear export of UBQLNs (Hirayama et al., 2018). UBQLN are central regulators of proteostasis and pathogenic variants in *UBQLN2*, as well as in *UBQLN4* and *UBQLN1*, have been linked to ALS or related neurodegenerative disorders (Deng et al., 2010; Edens et al., 2017; González-Pérez et al., 2012; Jachimowicz et al., 2019). Given this functional relationship, loss of DESI1 may compromise UBQLN trafficking and protein quality control, providing a plausible mechanism by which *DESI1* variants could contribute to ALS-like disease.

These findings reinforce the biological plausibility of *DESI1* as a novel ALS causative gene, providing both clinical and molecular evidence for its inclusion within the ALS spectrum.

4.2 Novelty and severity of DESI1 variants

To our knowledge*, DESI1* has never previously been implicated in human disease, making these findings the first to establish a clinical phenotype linked to its dysfunction. All variants identified in this study were extremely rare in the general population and predicted to be deleterious. The variant spectrum included frameshift, stop-gain,

nonsense, stop-loss, and splice-site variants, all of which are typically associated with severe loss-of-function consequences. These characteristics, together with segregation in affected families, strongly support their pathogenicity.

A noteworthy genotype–phenotype correlation emerged: the patient carrying the most truncated variant (*v5*) presented with juvenile-onset disease, whereas carriers of less severe truncating variants developed symptoms in adulthood. This observation suggests that mutation severity may influence disease onset and progression. Moreover, all variants identified to date mapped to the last three exons of DESI1, raising the possibility that earlier, more disruptive variants may result in embryonic lethality.

4.3 DESI1 Mutant Expression and Protein Stability

Our data revealed divergent effects of DESI1 mutations at the transcript level. For patient F1:II.2 (*v1*), qPCR indicated reduced transcript abundance, likely reflecting mRNA instability or degradation through nonsense-mediated decay. In contrast, patient F2:II.1 (*v2*) showed significantly increased transcript levels, possibly representing a compensatory response. Despite these differences, both mutations ultimately led to reduced DESI1 protein, underscoring that transcript fluctuations do not rescue protein expression.

Protein-level investigations provided further insights. Mutant DESI1 proteins (*v1, v2, v3, v4*) were consistently unstable and rapidly degraded via the proteasome, as evidenced by restoration upon MG-132 treatment. These results demonstrate that loss of protein stability is a common pathogenic mechanism across the identified variants. One plausible hypothesis is that protein misfolding triggers quality-control degradation pathways, preventing the accumulation of potentially toxic intermediates.

4.4 Functional Consequences of Defects in DESI1-UBQLN4 Interactions

DESI1 acts as a nuclear export adaptor for UBQLNs, mediating CRM1 recognition and subsequent nuclear export. Although DESI1 contains two NES domains, only NES2 is functionally active in CRM1 binding (Hirayama et al., 2018). In variants *v2*-*v5*, the complete loss of NES2 is expected to abolish CRM1 recognition, thereby blocking UBQLN nuclear export and leading to accumulation of polyubiquitinated proteins in the nucleus, where they may interfere with essential cellular processes. For variant *v1*, NES2

sequence remains intact, however exon 5 deletion likely induces conformational changes that may impair CRM1 recognition resulting in similar defects. Our ongoing Co-IP assays with CRM1 and DESI1-*v1* aim to assess this hypothesis.

The specific residues mediating DESI1-UBQLN interactions remain uncharacterized, yet our data showed unexpectedly increased binding between DESI1-*v1* and UBQLN4 compared to WT. Two mechanisms could explain this finding. First, the exon 5 skipping may create a "trapping mutant" that sequesters UBQLN4, and subsequent proteasomal degradation of DESI1-*v1* could then promote co-degradation of UBQLN4, reducing its functional pool. Second, given that DESI1 variants are rapidly targeted for degradation, UBQLN4 may recognize polyubiquitinated DESI1 through its UBA domain which binds polyubiquitin chains via hydrophobic interactions. This would result in persistent recruitment of UBQLN4 and enhance binding. Further experiments are underway to assess DESI1-v1 interactions with UBQLN1 and UBQLN2. Determining whether the aberrant binding is UBQLN4-specific or a general feature of *DESI1* variants will be critical for understanding the broader impact of DESI1 dysfunction on proteostasis in our patient.

4.5 Functional Implications of Variants within the PPPDE Domain of DESI1

The highly conserved PPPDE domain of DESI1 employs a cysteine-based catalytic dyad, distinguishing it from classical serine-based catalytic triads. Homodimerization is essential for DESI1 catalytic activity, with each monomer contributing key residues to form the composite His–Cys catalytic groove (Suh et al., 2012).

All *DESI1* variants identified in our cohort cluster within exons 4–6, which encodes the catalytic cysteine residue (Cys108). Variants *v1–v3* lack Cys108 and are therefore predicted to be catalytically inactive. Although *v4* variant preserves this residue, its severely altered C-terminal likely impairs homodimerization and substrate recognition.

Furthermore, our co-immunoprecipitation experiments revealed that *v1* not only lacks catalytic activity but also fails to bind SUMOylated BZEL, suggesting that sequence encoded by exon 5 contribute also to substrate recognition. Unlike SENP family deSUMOylases, which target a broad spectrum of substrates, DESI1 exhibits strict substrate specificity. Silencing of DESI1 does not affect global SUMOylation patterns (Shin et al., 2012). This restricted activity, together with the fact that DESI1 orthologs are

absent in lower eukaryotes whereas SENPs are universally conserved (Nayak and Müller, 2014), points to a specialized regulatory role for DESI1

To date only BZEL, a transcriptional repressor of BLIMP-1, has been validated as deSUMOylation substrate of DESI1. Interestingly, PPPDE domain also possesses S-depalmitoylase activity, although its physiological substrates have yet to be identified and are likely subject to similarly stringent substrate constraints.

Collectively, our findings suggest that through its PPPDE domain, DESI1 exerts specialized regulatory functions, particularly within the nucleus via deSUMOylation and S-depalmitoylation. Loss-of-function variants are therefore expected to disrupt tightly regulated pathways with major consequences for neuronal homeostasis.

4.6 Ongoing and Future Directions

Currently, we are extending our functional studies through co-immunoprecipitation assays of DESI1-*v1* with CRM1, as well as with UBQLN1 and UBQLN2. Immunofluorescence staining of UBQLN2 and UBQLN4, together with subcellular fractionation analyses, are also in progress to assess the impact of DESI1 variants on protein localization and trafficking.

To further explore the pathophysiological consequences of DESI1 loss-of-function, we are expanding the patient cohort and characterizing additional variants. In parallel, we are developing multiple disease models, including patient-derived iPSCs differentiated into motor neurons, CRISPR/Cas9-engineered neuronal cell lines and mutant zebrafish. These complementary systems will enable detailed dissection of downstream pathways affected by DESI1 dysfunction and may ultimately broaden the spectrum of ALS-associated genes.

4.7 Importance of the Study

Our findings identify *DESI1* as a novel ALS-associated candidate gene, providing new insights into the molecular mechanisms underlying ALS pathogenesis. By uncovering *DESI1*-related pathological alterations, this work supports the inclusion of *DESI1* in genetic diagnostic panels and underscores its potential as a future therapeutic target.

BIBLIOGRAPHY

Akçimen, F., Lopez, E. R., Landers, J. E., Nath, A., Chiò, A., Chia, R., & Traynor, B. J. (2023). Amyotrophic lateral sclerosis: translating genetic discoveries into therapies. Nature reviews. Genetics, 24(9), 642–658. https://doi.org/10.1038/s41576-023-00592-y

Al-Saif, A., Al-Mohanna, F., & Bohlega, S. (2011). A mutation in sigma-1 receptor causes juvenile amyotrophic lateral sclerosis. Annals of neurology, 70(6), 913–919. https://doi.org/10.1002/ana.22534

(2019). ALSUntangled No. 52: Glutathione. Amyotrophic Lateral Sclerosis and Frontotemporal Degeneration, 21(1–2), 154–157. https://doi.org/10.1080/21678421.2019.1697029

Atkinson, R., Leung, J., Bender, J., Kirkcaldie, M., Vickers, J., & King, A. (2021). TDP-43 mislocalization drives neurofilament changes in a novel model of TDP-43 proteinopathy. Disease models & mechanisms, 14(2), dmm047548. Advance online publication. https://doi.org/10.1242/dmm.047548

Ayala, Y. M., Zago, P., D'Ambrogio, A., Xu, Y. F., Petrucelli, L., Buratti, E., & Baralle, F. E. (2008). Structural determinants of the cellular localization and shuttling of TDP-43. Journal of cell science, 121(Pt 22), 3778–3785. https://doi.org/10.1242/jcs.038950

Bannwarth, S., Ait-El-Mkadem, S., Chaussenot, A., Genin, E. C., Lacas-Gervais, S., Fragaki, K., Berg-Alonso, L., Kageyama, Y., Serre, V., Moore, D. G., Verschueren, A., Rouzier, C., Le Ber, I., Augé, G., Cochaud, C., Lespinasse, F., N'Guyen, K., de Septenville, A., Brice, A., Yu-Wai-Man, P., … Paquis-Flucklinger, V. (2014). A mitochondrial origin for frontotemporal dementia and amyotrophic lateral sclerosis through CHCHD10 involvement. Brain : a journal of neurology, 137(Pt 8), 2329–2345. https://doi.org/10.1093/brain/awu138

Barsukova, A. G., Bourdette, D., & Forte, M. (2011). Mitochondrial calcium and its regulation in neurodegeneration induced by oxidative stress. The European journal of neuroscience, 34(3), 437–447. https://doi.org/10.1111/j.1460-9568.2011.07760.x

Belzil, V., Daoud, H., Camu, W. et al. Genetic analysis of SIGMAR1 as a cause of familial ALS with dementia. Eur J Hum Genet 21, 237–239 (2013). https://doi.org/10.1038/ejhg.2012.135

Brenner, D., Müller, K., Wieland, T., Weydt, P., Böhm, S., Lulé, D., Hübers, A., Neuwirth, C., Weber, M., Borck, G., Wahlqvist, M., Danzer, K. M., Volk, A. E., Meitinger, T., Strom, T. M., Otto, M., Kassubek, J., Ludolph, A. C., Andersen, P. M., & Weishaupt, J. H. (2016). NEK1 mutations in familial amyotrophic lateral sclerosis. Brain : a journal of neurology, 139(Pt 5), e28. https://doi.org/10.1093/brain/aww033

Carrì, M. T., Valle, C., Bozzo, F., & Cozzolino, M. (2015). Oxidative stress and mitochondrial damage: importance in non-SOD1 ALS. Frontiers in cellular neuroscience, 9, 41. https://doi.org/10.3389/fncel.2015.00041

Chance, P. F., Rabin, B. A., Ryan, S. G., Ding, Y., Scavina, M., Crain, B., Griffin, J. W., & Cornblath, D. R. (1998). Linkage of the gene for an autosomal dominant form of juvenile amyotrophic lateral sclerosis to chromosome 9q34. American journal of human genetics, 62(3), 633–640. https://doi.org/10.1086/301769

Chen, Y. Z., Bennett, C. L., Huynh, H. M., Blair, I. P., Puls, I., Irobi, J., Dierick, I., Abel, A., Kennerson, M. L., Rabin, B. A., Nicholson, G. A., Auer-Grumbach, M., Wagner, K., De Jonghe, P., Griffin, J. W., Fischbeck, K. H., Timmerman, V., Cornblath, D. R., & Chance, P. F. (2004). DNA/RNA helicase gene mutations in a form of juvenile amyotrophic lateral sclerosis (ALS4). American journal of human genetics, 74(6), 1128–1135. https://doi.org/10.1086/421054

Chi, L., Ke, Y., Luo, C., Gozal, D., & Liu, R. (2007). Depletion of reduced glutathione enhances motor neuron degeneration in vitro and in vivo. Neuroscience, 144(3), 991-1003.

Chow, C. Y., Landers, J. E., Bergren, S. K., Sapp, P. C., Grant, A. E., Jones, J. M., Everett, L., Lenk, G. M., McKenna-Yasek, D. M., Weisman, L. S., Figlewicz, D., Brown, R. H., & Meisler, M. H. (2009). Deleterious variants of FIG4, a phosphoinositide phosphatase, in patients with ALS. American journal of human genetics, 84(1), 85–88. https://doi.org/10.1016/j.ajhg.2008.12.010

Cooper-Knock, J., Walsh, M. J., Higginbottom, A., Robin Highley, J., Dickman, M. J., Edbauer, D., Ince, P. G., Wharton, S. B., Wilson, S. A., Kirby, J., Hautbergue, G. M., & Shaw, P. J. (2014). Sequestration of multiple RNA recognition motif-

containing proteins by C9orf72 repeat expansions. Brain : a journal of neurology, 137(Pt 7), 2040–2051. https://doi.org/10.1093/brain/awu120

Cooper-Knock, J., Moll, T., Ramesh, T., Castelli, L., Beer, A., Robins, H., Fox, I., Niedermoser, I., Van Damme, P., Moisse, M., Robberecht, W., Hardiman, O., Panades, M. P., Assialioui, A., Mora, J. S., Basak, A. N., Morrison, K. E., Shaw, C. E., Al-Chalabi, A., Landers, J. E., … Shaw, P. J. (2019). Mutations in the Glycosyltransferase Domain of GLT8D1 Are Associated with Familial Amyotrophic Lateral Sclerosis. Cell reports, 26(9), 2298–2306.e5. https://doi.org/10.1016/j.celrep.2019.02.006

Corrado, L., Carlomagno, Y., Falasco, L., Mellone, S., Godi, M., Cova, E., Cereda, C., Testa, L., Mazzini, L., & D'Alfonso, S. (2011). A novel peripherin gene (PRPH) mutation identified in one sporadic amyotrophic lateral sclerosis patient. Neurobiology of aging, 32(3), 552.e1–552.e5526. https://doi.org/10.1016/j.neurobiolaging.2010.02.011

DeJesus-Hernandez, M., Mackenzie, I. R., Boeve, B. F., Boxer, A. L., Baker, M., Rutherford, N. J., Nicholson, A. M., Finch, N. A., Flynn, H., Adamson, J., Kouri, N., Wojtas, A., Sengdy, P., Hsiung, G. Y., Karydas, A., Seeley, W. W., Josephs, K. A., Coppola, G., Geschwind, D. H., Wszolek, Z. K., … Rademakers, R. (2011). Expanded GGGGCC hexanucleotide repeat in noncoding region of C9ORF72 causes chromosome 9p-linked FTD and ALS. Neuron, 72(2), 245–256. https://doi.org/10.1016/j.neuron.2011.09.011

Deng, H.-X., Zhai, H., Bigio, E.H., Yan, J., Fecto, F., Ajroud, K., Mishra, M., Ajroud-Driss, S., Heller, S., Sufit, R., Siddique, N., Mugnaini, E. and Siddique, T. (2010), FUS-immunoreactive inclusions are a common feature in sporadic and non-SOD1 familial amyotrophic lateral sclerosis. Ann Neurol., 67: 739-748. https://doi.org/10.1002/ana.22051

Deng, H. X., Chen, W., Hong, S. T., Boycott, K. M., Gorrie, G. H., Siddique, N., Yang, Y., Fecto, F., Shi, Y., Zhai, H., Jiang, H., Hirano, M., Rampersaud, E., Jansen, G. H., Donkervoort, S., Bigio, E. H., Brooks, B. R., Ajroud, K., Sufit, R. L., Haines, J. L., … Siddique, T. (2011). Mutations in UBQLN2 cause dominant X-linked juvenile and adult-onset ALS and ALS/dementia. Nature, 477(7363), 211–215. https://doi.org/10.1038/nature10353

Edens, B. M., Yan, J., Miller, N., Deng, H. X., Siddique, T., & Ma, Y. C. (2017). A novel ALS-associated variant in UBQLN4 regulates motor axon morphogenesis. eLife, 6, e25453. https://doi.org/10.7554/eLife.25453

Elden, A. C., Kim, H. J., Hart, M. P., Chen-Plotkin, A. S., Johnson, B. S., Fang, X., Armakola, M., Geser, F., Greene, R., Lu, M. M., Padmanabhan, A., Clay-Falcone, D., McCluskey, L., Elman, L., Juhr, D., Gruber, P. J., Rüb, U., Auburger, G., Trojanowski, J. Q., Lee, V. M., … Gitler, A. D. (2010). Ataxin-2 intermediate-length polyglutamine expansions are associated with increased risk for ALS. Nature, 466(7310), 1069–1075. https://doi.org/10.1038/nature09320

Fang, X., Lin, H., Wang, X., Zuo, Q., Qin, J., & Zhang, P. (2015). The NEK1 interactor, C21ORF2, is required for efficient DNA damage repair. Acta biochimica et biophysica Sinica, 47(10), 834–841. https://doi.org/10.1093/abbs/gmv076

Farhan, S. M. K., Howrigan, D. P., Abbott, L. E., Klim, J. R., Topp, S. D., Byrnes, A. E., Churchhouse, C., Phatnani, H., Smith, B. N., Rampersaud, E., Wu, G., Wuu, J., Shatunov, A., Iacoangeli, A., Al Khleifat, A., Mordes, D. A., Ghosh, S., ALSGENS Consortium, FALS Consortium, Project MinE Consortium, … Neale, B. M. (2019). Exome sequencing in amyotrophic lateral sclerosis implicates a novel gene, DNAJC7, encoding a heat-shock protein. Nature neuroscience, 22(12), 1966–1974. https://doi.org/10.1038/s41593-019-0530-0

Fecto, F., Yan, J., Vemula, S. P., Liu, E., Yang, Y., Chen, W., Zheng, J. G., Shi, Y., Siddique, N., Arrat, H., Donkervoort, S., Ajroud-Driss, S., Sufit, R. L., Heller, S. L., Deng, H. X., & Siddique, T. (2011). SQSTM1 mutations in familial and sporadic amyotrophic lateral sclerosis. Archives of neurology, 68(11), 1440–1446. https://doi.org/10.1001/archneurol.2011.250

Freischmidt, A., Wieland, T., Richter, B., Ruf, W., Schaeffer, V., Müller, K., Marroquin, N., Nordin, F., Hübers, A., Weydt, P., Pinto, S., Press, R., Millecamps, S., Molko, N., Bernard, E., Desnuelle, C., Soriani, M. H., Dorst, J., Graf, E., Nordström, U., … Weishaupt, J. H. (2015). Haploinsufficiency of TBK1 causes familial ALS and fronto-temporal dementia. Nature neuroscience, 18(5), 631–636. https://doi.org/10.1038/nn.4000

Gerson, J.E., Linton, H., Xing, J. et al. Shared and divergent phase separation and aggregation properties of brain-expressed ubiquilins. Sci Rep 11, 287 (2021). https://doi.org/10.1038/s41598-020-78775-4

González-Pérez, P., Lu, Y., Chian, R. J., Sapp, P. C., Tanzi, R. E., Bertram, L., McKenna-Yasek, D., Gao, F. B., & Brown, R. H., Jr (2012). Association of UBQLN1 mutation with Brown-Vialetto-Van Laere syndrome but not typical ALS. Neurobiology of disease, 48(3), 391–398. https://doi.org/10.1016/j.nbd.2012.06.018

Greenway, M. J., Andersen, P. M., Russ, C., Ennis, S., Cashman, S., Donaghy, C., Patterson, V., Swingler, R., Kieran, D., Prehn, J., Morrison, K. E., Green, A., Acharya, K. R., Brown, R. H., Jr, & Hardiman, O. (2006). ANG mutations segregate with familial and 'sporadic' amyotrophic lateral sclerosis. Nature genetics, 38(4), 411–413. https://doi.org/10.1038/ng1742

Guo, C., Sun, L., Chen, X., & Zhang, D. (2013). Oxidative stress, mitochondrial damage and neurodegenerative diseases. Neural regeneration research, 8(21), 2003–2014. https://doi.org/10.3969/j.issn.1673-5374.2013.21.009

Hadano, S., Hand, C. K., Osuga, H., Yanagisawa, Y., Otomo, A., Devon, R. S., Miyamoto, N., Showguchi-Miyata, J., Okada, Y., Singaraja, R., Figlewicz, D. A., Kwiatkowski, T., Hosler, B. A., Sagie, T., Skaug, J., Nasir, J., Brown, R. H., Jr, Scherer, S. W., Rouleau, G. A., Hayden, M. R., … Ikeda, J. E. (2001). A gene encoding a putative GTPase regulator is mutated in familial amyotrophic lateral sclerosis 2. Nature genetics, 29(2), 166–173. https://doi.org/10.1038/ng1001-166

Hardiman, O., Al-Chalabi, A., Chio, A. et al. Amyotrophic lateral sclerosis. Nat Rev Dis Primers 3, 17071 (2017). https://doi.org/10.1038/nrdp.2017.71

Harrison, A. F., & Shorter, J. (2017). RNA-binding proteins with prion-like domains in health and disease. The Biochemical journal, 474(8), 1417–1438. https://doi.org/10.1042/BCJ20160499

Hemerková, P., & Vališ, M. (2021). Role of Oxidative Stress in the Pathogenesis of Amyotrophic Lateral Sclerosis: Antioxidant Metalloenzymes and Therapeutic Strategies. Biomolecules, 11(3), 437. https://doi.org/10.3390/biom11030437

Hipp, M. S., Kasturi, P., & Hartl, F. U. (2019). The proteostasis network and its decline in ageing. Nature reviews. Molecular cell biology, 20(7), 421–435. https://doi.org/10.1038/s41580-019-0101-y

Hirayama, S., Sugihara, M., Morito, D., Iemura, S. I., Natsume, T., Murata, S., & Nagata, K. (2018). Nuclear export of ubiquitinated proteins via the UBIN-POST

system. Proceedings of the National Academy of Sciences of the United States of America, 115(18), E4199–E4208. https://doi.org/10.1073/pnas.1711017115

Hjerpe, R., Bett, J. S., Keuss, M. J., Solovyova, A., McWilliams, T. G., Johnson, C., Sahu, I., Varghese, J., Wood, N., Wightman, M., Osborne, G., Bates, G. P., Glickman, M. H., Trost, M., Knebel, A., Marchesi, F., & Kurz, T. (2016). UBQLN2 Mediates Autophagy-Independent Protein Aggregate Clearance by the Proteasome. Cell, 166(4), 935–949. https://doi.org/10.1016/j.cell.2016.07.001

Jachimowicz, R. D., Beleggia, F., Isensee, J., Velpula, B. B., Goergens, J., Bustos, M. A., Doll, M. A., Shenoy, A., Checa-Rodriguez, C., Wiederstein, J. L., Baranes-Bachar, K., Bartenhagen, C., Hertwig, F., Teper, N., Nishi, T., Schmitt, A., Distelmaier, F., Lüdecke, H. J., Albrecht, B., Krüger, M., … Shiloh, Y. (2019). UBQLN4 Represses Homologous Recombination and Is Overexpressed in Aggressive Tumors. Cell, 176(3), 505–519.e22. https://doi.org/10.1016/j.cell.2018.11.024

Johnson, J. O., Mandrioli, J., Benatar, M., Abramzon, Y., Van Deerlin, V. M., Trojanowski, J. Q., Gibbs, J. R., Brunetti, M., Gronka, S., Wuu, J., Ding, J., McCluskey, L., Martinez-Lage, M., Falcone, D., Hernandez, D. G., Arepalli, S., Chong, S., Schymick, J. C., Rothstein, J., Landi, F., … Traynor, B. J. (2010). Exome sequencing reveals VCP mutations as a cause of familial ALS. Neuron, 68(5), 857–864. https://doi.org/10.1016/j.neuron.2010.11.036

Johnson, J. O., Pioro, E. P., Boehringer, A., Chia, R., Feit, H., Renton, A. E., Pliner, H. A., Abramzon, Y., Marangi, G., Winborn, B. J., Gibbs, J. R., Nalls, M. A., Morgan, S., Shoai, M., Hardy, J., Pittman, A., Orrell, R. W., Malaspina, A., Sidle, K. C., Fratta, P., … Traynor, B. J. (2014). Mutations in the Matrin 3 gene cause familial amyotrophic lateral sclerosis. Nature neuroscience, 17(5), 664–666. https://doi.org/10.1038/nn.3688

Kabashi, E., Valdmanis, P. N., Dion, P., Spiegelman, D., McConkey, B. J., Vande Velde, C., Bouchard, J. P., Lacomblez, L., Pochigaeva, K., Salachas, F., Pradat, P. F., Camu, W., Meininger, V., Dupre, N., & Rouleau, G. A. (2008). TARDBP mutations in individuals with sporadic and familial amyotrophic lateral sclerosis. Nature genetics, 40(5), 572–574. https://doi.org/10.1038/ng.132

Kannan, A., Cuartas, J., Gangwani, P., Branzei, D., & Gangwani, L. (2022). Mutation in senataxin alters the mechanism of R-loop resolution in amyotrophic lateral

sclerosis 4. Brain : a journal of neurology, 145(9), 3072–3094. https://doi.org/10.1093/brain/awab464

Kim, H. J., Kim, N. C., Wang, Y. D., Scarborough, E. A., Moore, J., Diaz, Z., MacLea, K. S., Freibaum, B., Li, S., Molliex, A., Kanagaraj, A. P., Carter, R., Boylan, K. B., Wojtas, A. M., Rademakers, R., Pinkus, J. L., Greenberg, S. A., Trojanowski, J. Q., Traynor, B. J., Smith, B. N., … Taylor, J. P. (2013). Mutations in prion-like domains in hnRNPA2B1 and hnRNPA1 cause multisystem proteinopathy and ALS. Nature, 495(7442), 467–473. https://doi.org/10.1038/nature11922

Kume, K., Kurashige, T., Muguruma, K., Morino, H., Tada, Y., Kikumoto, M., Miyamoto, T., Akutsu, S. N., Matsuda, Y., Matsuura, S., Nakamori, M., Nishiyama, A., Izumi, R., Niihori, T., Ogasawara, M., Eura, N., Kato, T., Yokomura, M., Nakayama, Y., Ito, H., … Kawakami, H. (2023). CGG repeat expansion in LRP12 in amyotrophic lateral sclerosis. American journal of human genetics, 110(7), 1086–1097. https://doi.org/10.1016/j.ajhg.2023.05.014

Kwiatkowski, T. J., Jr, Bosco, D. A., Leclerc, A. L., Tamrazian, E., Vanderburg, C. R., Russ, C., Davis, A., Gilchrist, J., Kasarskis, E. J., Munsat, T., Valdmanis, P., Rouleau, G. A., Hosler, B. A., Cortelli, P., de Jong, P. J., Yoshinaga, Y., Haines, J. L., Pericak-Vance, M. A., Yan, J., Ticozzi, N., … Brown, R. H., Jr (2009). Mutations in the FUS/TLS gene on chromosome 16 cause familial amyotrophic lateral sclerosis. Science (New York, N.Y.), 323(5918), 1205–1208. https://doi.org/10.1126/science.1166066

Lin, F., Lin, W., Zhu, C., Lin, J., Zhu, J., Li, X. Y., Wang, Z., Wang, C., & Huang, H. (2021). Sequencing of neurofilament genes identified NEFH Ser787Arg as a novel risk variant of sporadic amyotrophic lateral sclerosis in Chinese subjects. BMC medical genomics, 14(1), 222. https://doi.org/10.1186/s12920-021-01073-z

Lin, B.C., Higgins, N.R., Phung, T.H. and Monteiro, M.J. (2022), UBQLN proteins in health and disease with a focus on UBQLN2 in ALS/FTD. FEBS J, 289: 6132-6153. https://doi.org/10.1111/febs.16129

Ling, S. C., Polymenidou, M., & Cleveland, D. W. (2013). Converging mechanisms in ALS and FTD: disrupted RNA and protein homeostasis. Neuron, 79(3), 416–438. https://doi.org/10.1016/j.neuron.2013.07.033

Luebben, A. V., Bender, D., Becker, S., Crowther, L. M., Erven, I., Hofmann, K., Söding, J., Klemp, H., Bellotti, C., Stäuble, A., Qiu, T., Kathayat, R. S., Dickinson, B. C., Gärtner, J., Sheldrick, G. M., Krätzner, R., & Steinfeld, R. (2022). Cln5 represents a new type of cysteine-based S-depalmitoylase linked to neurodegeneration. Science advances, 8(15), eabj8633. https://doi.org/10.1126/sciadv.abj8633

Mackenzie, I. R., Nicholson, A. M., Sarkar, M., Messing, J., Purice, M. D., Pottier, C., Annu, K., Baker, M., Perkerson, R. B., Kurti, A., Matchett, B. J., Mittag, T., Temirov, J., Hsiung, G. R., Krieger, C., Murray, M. E., Kato, M., Fryer, J. D., Petrucelli, L., Zinman, L., … Rademakers, R. (2017). TIA1 Mutations in Amyotrophic Lateral Sclerosis and Frontotemporal Dementia Promote Phase Separation and Alter Stress Granule Dynamics. Neuron, 95(4), 808–816.e9. https://doi.org/10.1016/j.neuron.2017.07.025

Marín I. (2014). The ubiquilin gene family: evolutionary patterns and functional insights. BMC evolutionary biology, 14, 63. https://doi.org/10.1186/1471-2148-14-63

Maruyama, H., Morino, H., Ito, H., Izumi, Y., Kato, H., Watanabe, Y., Kinoshita, Y., Kamada, M., Nodera, H., Suzuki, H., Komure, O., Matsuura, S., Kobatake, K., Morimoto, N., Abe, K., Suzuki, N., Aoki, M., Kawata, A., Hirai, T., Kato, T., … Kawakami, H. (2010). Mutations of optineurin in amyotrophic lateral sclerosis. Nature, 465(7295), 223–226. https://doi.org/10.1038/nature08971

Matsumoto, G., Shimogori, T., Hattori, N., & Nukina, N. (2015). TBK1 controls autophagosomal engulfment of polyubiquitinated mitochondria through p62/SQSTM1 phosphorylation. Human molecular genetics, 24(15), 4429–4442. https://doi.org/10.1093/hmg/ddv179

McAlary, L., Plotkin, S. S., Yerbury, J. J., & Cashman, N. R. (2019). Prion-like propagation of protein misfolding and aggregation in amyotrophic lateral sclerosis. Frontiers in molecular neuroscience, 12, 262.

Mead, R. J., Shan, N., Reiser, H. J., Marshall, F., & Shaw, P. J. (2023). Amyotrophic lateral sclerosis: a neurodegenerative disorder poised for successful therapeutic translation. Nature reviews. Drug discovery, 22(3), 185–212. https://doi.org/10.1038/s41573-022-00612-2

Mohassel, P., Donkervoort, S., Lone, M. A., Nalls, M., Gable, K., Gupta, S. D., Foley, A. R., Hu, Y., Saute, J. A. M., Moreira, A. L., Kok, F., Introna, A., Logroscino, G., Grunseich, C., Nickolls, A. R., Pourshafie, N., Neuhaus, S. B., Saade, D., Gangfuß, A., Kölbel, H., … Bönnemann, C. G. (2021). Childhood amyotrophic lateral sclerosis caused by excess sphingolipid synthesis. Nature medicine, 27(7), 1197–1204. https://doi.org/10.1038/s41591-021-01346-1

Nayak, A., & Müller, S. (2014). SUMO-specific proteases/isopeptidases: SENPs and beyond. Genome biology, 15(7), 422. https://doi.org/10.1186/s13059-014-0422-2

Nicolas, A., Kenna, K. P., Renton, A. E., Ticozzi, N., Faghri, F., Chia, R., Dominov, J. A., Kenna, B. J., Nalls, M. A., Keagle, P., Rivera, A. M., van Rheenen, W., Murphy, N. A., van Vugt, J. J. F. A., Geiger, J. T., Van der Spek, R. A., Pliner, H. A., Shankaracharya, Smith, B. N., Marangi, G., … Landers, J. E. (2018). Genome-wide Analyses Identify KIF5A as a Novel ALS Gene. Neuron, 97(6), 1267–1288. https://doi.org/10.1016/j.neuron.2018.02.027

Nishimura, A. L., Mitne-Neto, M., Silva, H. C., Richieri-Costa, A., Middleton, S., Cascio, D., Kok, F., Oliveira, J. R., Gillingwater, T., Webb, J., Skehel, P., & Zatz, M. (2004). A mutation in the vesicle-trafficking protein VAPB causes late-onset spinal muscular atrophy and amyotrophic lateral sclerosis. American journal of human genetics, 75(5), 822–831. https://doi.org/10.1086/425287

Parkinson, N., Ince, P. G., Smith, M. O., Highley, R., Skibinski, G., Andersen, P. M., Morrison, K. E., Pall, H. S., Hardiman, O., Collinge, J., Shaw, P. J., Fisher, E. M., MRC Proteomics in ALS Study, & FReJA Consortium (2006). ALS phenotypes with mutations in CHMP2B (charged multivesicular body protein 2B). Neurology, 67(6), 1074–1077. https://doi.org/10.1212/01.wnl.0000231510.89311.8b

Parzych, K. R., & Klionsky, D. J. (2014). An overview of autophagy: morphology, mechanism, and regulation. Antioxidants & redox signaling, 20(3), 460–473. https://doi.org/10.1089/ars.2013.5371

Pedrini, S., Sau, D., Guareschi, S., Bogush, M., Brown, R. H., Jr, Naniche, N., Kia, A., Trotti, D., & Pasinelli, P. (2010). ALS-linked mutant SOD1 damages mitochondria by promoting conformational changes in Bcl-2. Human molecular genetics, 19(15), 2974–2986. https://doi.org/10.1093/hmg/ddq202

Provenzano, F., Torazza, C., Bonifacino, T., Bonanno, G., & Milanese, M. (2023). The Key Role of Astrocytes in Amyotrophic Lateral Sclerosis and Their Commitment to Glutamate Excitotoxicity. International journal of molecular sciences, 24(20), 15430. https://doi.org/10.3390/ijms242015430

Puls, I., Jonnakuty, C., LaMonte, B. H., Holzbaur, E. L., Tokito, M., Mann, E., Floeter, M. K., Bidus, K., Drayna, D., Oh, S. J., Brown, R. H., Jr, Ludlow, C. L., & Fischbeck, K. H. (2003). Mutant dynactin in motor neuron disease. Nature genetics, 33(4), 455–456. https://doi.org/10.1038/ng1123

Renaud, L., Picher-Martel, V., Codron, P., & Julien, J. P. (2019). Key role of UBQLN2 in pathogenesis of amyotrophic lateral sclerosis and frontotemporal dementia. Acta neuropathologica communications, 7(1), 103. https://doi.org/10.1186/s40478-019-0758-7

Richter, B., Sliter, D. A., Herhaus, L., Stolz, A., Wang, C., Beli, P., Zaffagnini, G., Wild, P., Martens, S., Wagner, S. A., Youle, R. J., & Dikic, I. (2016). Phosphorylation of OPTN by TBK1 enhances its binding to Ub chains and promotes selective autophagy of damaged mitochondria. Proceedings of the National Academy of Sciences of the United States of America, 113(15), 4039–4044. https://doi.org/10.1073/pnas.1523926113

Rosen, D. R., Siddique, T., Patterson, D., Figlewicz, D. A., Sapp, P., Hentati, A., Donaldson, D., Goto, J., O'Regan, J. P., & Deng, H. X. (1993). Mutations in Cu/Zn superoxide dismutase gene are associated with familial amyotrophic lateral sclerosis. Nature, 362(6415), 59–62. https://doi.org/10.1038/362059a0

Shin, E. J., Shin, H. M., Nam, E., Kim, W. S., Kim, J. H., Oh, B. H., & Yun, Y. (2012). DeSUMOylating isopeptidase: a second class of SUMO protease. EMBO reports, 13(4), 339–346. https://doi.org/10.1038/embor.2012.3

Singh, A., Kukreti, R., Saso, L., & Kukreti, S. (2019). Oxidative Stress: A Key Modulator in Neurodegenerative Diseases. Molecules, 24(8), 1583. https://doi.org/10.3390/molecules24081583

Smith, B. N., Ticozzi, N., Fallini, C., Gkazi, A. S., Topp, S., Kenna, K. P., Scotter, E. L., Kost, J., Keagle, P., Miller, J. W., Calini, D., Vance, C., Danielson, E. W., Troakes, C., Tiloca, C., Al-Sarraj, S., Lewis, E. A., King, A., Colombrita, C., Pensato, V., … Landers, J. E. (2014). Exome-wide rare variant analysis

identifies TUBA4A mutations associated with familial ALS. Neuron, 84(2), 324–331. https://doi.org/10.1016/j.neuron.2014.09.027

Smith, B. N., Topp, S. D., Fallini, C., Shibata, H., Chen, H. J., Troakes, C., King, A., Ticozzi, N., Kenna, K. P., Soragia-Gkazi, A., Miller, J. W., Sato, A., Dias, D. M., Jeon, M., Vance, C., Wong, C. H., de Majo, M., Kattuah, W., Mitchell, J. C., Scotter, E. L., … Shaw, C. E. (2017). Mutations in the vesicular trafficking protein annexin A11 are associated with amyotrophic lateral sclerosis. Science translational medicine, 9(388), eaad9157. https://doi.org/10.1126/scitranslmed.aad9157

Stoica, R., De Vos, K. J., Paillusson, S., Mueller, S., Sancho, R. M., Lau, K. F., Vizcay-Barrena, G., Lin, W. L., Xu, Y. F., Lewis, J., Dickson, D. W., Petrucelli, L., Mitchell, J. C., Shaw, C. E., & Miller, C. C. (2014). ER-mitochondria associations are regulated by the VAPB-PTPIP51 interaction and are disrupted by ALS/FTD-associated TDP-43. Nature communications, 5, 3996. https://doi.org/10.1038/ncomms4996

Suh, H. Y., Kim, J. H., Woo, J. S., Ku, B., Shin, E. J., Yun, Y., & Oh, B. H. (2012). Crystal structure of DeSI-1, a novel deSUMOylase belonging to a putative isopeptidase superfamily. Proteins, 80(8), 2099–2104. https://doi.org/10.1002/prot.24093

Suk, T.R., Rousseaux, M.W.C. The role of TDP-43 mislocalization in amyotrophic lateral sclerosis. Mol Neurodegeneration 15, 45 (2020). https://doi.org/10.1186/s13024-020-00397-1

Synofzik, M., Maetzler, W., Grehl, T., Prudlo, J., Vom Hagen, J. M., Haack, T., Rebassoo, P., Munz, M., Schöls, L., & Biskup, S. (2012). Screening in ALS and FTD patients reveals 3 novel UBQLN2 mutations outside the PXX domain and a pure FTD phenotype. Neurobiology of aging, 33(12), 2949.e13–2949.e2.949E17. https://doi.org/10.1016/j.neurobiolaging.2012.07.002

Şentürk, M., Lin, G., Zuo, Z., Mao, D., Watson, E., Mikos, A. G., & Bellen, H. J. (2019). Ubiquilins regulate autophagic flux through mTOR signalling and lysosomal acidification. Nature cell biology, 21(3), 384–396. https://doi.org/10.1038/s41556-019-0281-x

Tafuri, F., Ronchi, D., Magri, F., Comi, G. P., & Corti, S. (2015). SOD1 misplacing and mitochondrial dysfunction in amyotrophic lateral sclerosis pathogenesis.

Frontiers in cellular neuroscience, 9, 336. https://doi.org/10.3389/fncel.2015.00336

Takahashi, Y., Fukuda, Y., Yoshimura, J., Toyoda, A., Kurppa, K., Moritoyo, H., Belzil, V. V., Dion, P. A., Higasa, K., Doi, K., Ishiura, H., Mitsui, J., Date, H., Ahsan, B., Matsukawa, T., Ichikawa, Y., Moritoyo, T., Ikoma, M., Hashimoto, T., Kimura, F., … Tsuji, S. (2013). ERBB4 mutations that disrupt the neuregulin-ErbB4 pathway cause amyotrophic lateral sclerosis type 19. American journal of human genetics, 93(5), 900–905. https://doi.org/10.1016/j.ajhg.2013.09.008

Taylor, J. P., Brown, R. H., Jr, & Cleveland, D. W. (2016). Decoding ALS: from genes to mechanism. Nature, 539(7628), 197–206. https://doi.org/10.1038/nature20413

Theunissen, F., West, P.K., Brennan, S. et al. New perspectives on cytoskeletal dysregulation and mitochondrial mislocalization in amyotrophic lateral sclerosis. Transl Neurodegener 10, 46 (2021). https://doi.org/10.1186/s40035-021-00272-z

Tompson, S. W., & Young, T. L. (2017). Assaying the Effects of Splice Site Variants by Exon Trapping in a Mammalian Cell Line. Bio-protocol, 7(10), e2281. https://doi.org/10.21769/BioProtoc.2281

Van Deerlin, V. M., Leverenz, J. B., Bekris, L. M., Bird, T. D., Yuan, W., Elman, L. B., Clay, D., Wood, E. M., Chen-Plotkin, A. S., Martinez-Lage, M., Steinbart, E., McCluskey, L., Grossman, M., Neumann, M., Wu, I. L., Yang, W. S., Kalb, R., Galasko, D. R., Montine, T. J., Trojanowski, J. Q., … Yu, C. E. (2008). TARDBP mutations in amyotrophic lateral sclerosis with TDP-43 neuropathology: a genetic and histopathological analysis. The Lancet. Neurology, 7(5), 409–416. https://doi.org/10.1016/S1474-4422(08)70071-1

van Rheenen, W., Shatunov, A., Dekker, A. M., McLaughlin, R. L., Diekstra, F. P., Pulit, S. L., van der Spek, R. A., Võsa, U., de Jong, S., Robinson, M. R., Yang, J., Fogh, I., van Doormaal, P. T., Tazelaar, G. H., Koppers, M., Blokhuis, A. M., Sproviero, W., Jones, A. R., Kenna, K. P., van Eijk, K. R., … Veldink, J. H. (2016). Genome-wide association analyses identify new risk variants and the genetic architecture of amyotrophic lateral sclerosis. Nature genetics, 48(9), 1043–1048. https://doi.org/10.1038/ng.3622

Wang, S., Tatman, M., & Monteiro, M. J. (2020). Overexpression of UBQLN1 reduces neuropathology in the P497S UBQLN2 mouse model of ALS/FTD. Acta

neuropathologica communications, 8(1), 164. https://doi.org/10.1186/s40478-020-01039-9

Wang, H., Guan, L., & Deng, M. (2023). Recent progress of the genetics of amyotrophic lateral sclerosis and challenges of gene therapy. Frontiers in neuroscience, 17, 1170996. https://doi.org/10.3389/fnins.2023.1170996

Williams, K. L., Topp, S., Yang, S., Smith, B., Fifita, J. A., Warraich, S. T., Zhang, K. Y., Farrawell, N., Vance, C., Hu, X., Chesi, A., Leblond, C. S., Lee, A., Rayner, S. L., Sundaramoorthy, V., Dobson-Stone, C., Molloy, M. P., van Blitterswijk, M., Dickson, D. W., Petersen, R. C., … Blair, I. P. (2016). CCNF mutations in amyotrophic lateral sclerosis and frontotemporal dementia. Nature communications, 7, 11253. https://doi.org/10.1038/ncomms11253

Wilson, D. M., 3rd, Cookson, M. R., Van Den Bosch, L., Zetterberg, H., Holtzman, D. M., & Dewachter, I. (2023). Hallmarks of neurodegenerative diseases. Cell, 186(4), 693–714. https://doi.org/10.1016/j.cell.2022.12.032

Wu, C. H., Fallini, C., Ticozzi, N., Keagle, P. J., Sapp, P. C., Piotrowska, K., Lowe, P., Koppers, M., McKenna-Yasek, D., Baron, D. M., Kost, J. E., Gonzalez-Perez, P., Fox, A. D., Adams, J., Taroni, F., Tiloca, C., Leclerc, A. L., Chafe, S. C., Mangroo, D., Moore, M. J., … Landers, J. E. (2012). Mutations in the profilin 1 gene cause familial amyotrophic lateral sclerosis. Nature, 488(7412), 499–503. https://doi.org/10.1038/nature11280

Yang, Y., Hentati, A., Deng, H. X., Dabbagh, O., Sasaki, T., Hirano, M., Hung, W. Y., Ouahchi, K., Yan, J., Azim, A. C., Cole, N., Gascon, G., Yagmour, A., Ben-Hamida, M., Pericak-Vance, M., Hentati, F., & Siddique, T. (2001). The gene encoding alsin, a protein with three guanine-nucleotide exchange factor domains, is mutated in a form of recessive amyotrophic lateral sclerosis. Nature genetics, 29(2), 160–165. https://doi.org/10.1038/ng1001-160

Yu, Y., Pang, D., Huang, J. et al. Downregulation of Lnc-ABCA12-3 modulates UBQLN1 expression and protein homeostasis pathways in amyotrophic lateral sclerosis. Sci Rep 14, 21383 (2024). https://doi.org/10.1038/s41598-024-72666-8

Zelina, P., de Ruiter, A. A., Kolsteeg, C., van Ginneken, I., Vos, H. R., Supiot, L. F., Burgering, B. M. T., Meye, F. J., Veldink, J. H., van den Berg, L. H., & Pasterkamp, R. J. (2024). ALS-associated C21ORF2 variant disrupts DNA

damage repair, mitochondrial metabolism, neuronal excitability and NEK1 levels in human motor neurons. Acta neuropathologica communications, 12(1), 144. https://doi.org/10.1186/s40478-024-01852-6

Zhang, K., Donnelly, C. J., Haeusler, A. R., Grima, J. C., Machamer, J. B., Steinwald, P., Daley, E. L., Miller, S. J., Cunningham, K. M., Vidensky, S., Gupta, S., Thomas, M. A., Hong, I., Chiu, S. L., Huganir, R. L., Ostrow, L. W., Matunis, M. J., Wang, J., Sattler, R., Lloyd, T. E., … Rothstein, J. D. (2015). The C9orf72 repeat expansion disrupts nucleocytoplasmic transport. Nature, 525(7567), 56–61. https://doi.org/10.1038/nature14973

Zheng, T., Yang, Y., & Castañeda, C. A. (2020). Structure, dynamics and functions of UBQLNs: at the crossroads of protein quality control machinery. Biochemical Journal, 477(18), 3471-3497.